energies

MDPI

Article

Subsalt Rotliegend Sediments—A New Challenge for Geothermal Systems in Poland

Rafał Kudrewicz [1], Bartosz Papiernik [2,*], Marek Hajto [2] and Grzegorz Machowski [2]

[1] Polish Oil and Gas Company, 01-224 Warszawa, Poland; rafal.kudrewicz@pgnig.pl
[2] Faculty of Geology, Geophysics and Environmental Protection, AGH University of Science and Technology, 30-059 Krakow, Poland; mhajto@agh.edu.pl (M.H.); machog@agh.edu.pl (G.M.)
* Correspondence: papiernik@agh.edu.pl

Abstract: New seismic data and the completion of the K-1 petroleum exploratory well, located close to the axial zone of the Mogilno-Łódź Trough (Polish Lowlands) delivered new insight into local structural, tectonic, facial and thermal variability of this geological unit. In this paper, the two variants of 3D models (SMV1 and SMV2) of Permian-Mesozoic strata are presented for the salt pillow related Kłecko Anticline, while resources assessment was confined to the Rotliegend Enhanced Geothermal System (EGS) type reservoir, that is divided into Playa, Eolian and Fluvial facies-based complexes. Using very conservative assumptions on the methods of the EGS reservoir development, authors assessed that heat in place and technical potential for eolian sandstones are about 386 PJ and ca. 2814 kW, respectively, and for Fluvial 367 PJ and ca. 2850 kW in relation to the volume of 1 km^3 at depths of about 5000 m b.s.l. The authors recommend for the further development of the Eolian complex because of its low shale content, influencing the high susceptibility to fracking. The presented research is the first Polish local resources assessment for an EGS reservoir in sedimentary Rotliegend, within thermal anomaly below the salt pillow, which is one of over 100 salt structures mapped in Poland.

Keywords: Rotliegend; 3D geological modeling; thermal conductivity; EGS

check for updates

Citation: Kudrewicz, R.; Papiernik, B.; Hajto, M.; Machowski, G. Subsalt Rotliegend Sediments—A New Challenge for Geothermal Systems in Poland. *Energies* **2022**, *15*, 1166. https://doi.org/10.3390/en15031166

Academic Editor: Carlo Roselli

Received: 4 December 2021
Accepted: 24 January 2022
Published: 4 February 2022

Publisher's Note: MDPI stays neutral with regard to jurisdictional claims in published maps and institutional affiliations.

Copyright: © 2022 by the authors. Licensee MDPI, Basel, Switzerland. This article is an open access article distributed under the terms and conditions of the Creative Commons Attribution (CC BY) license (https://creativecommons.org/licenses/by/4.0/).

1. Introduction

Geothermal research started in the Polish Lowland over 40 years ago and has resulted in the discovery of two low-temperature prospecting reservoirs: Lower Cretaceous and Lower Jurassic located within Mogilno-Łódź Trough, Szczecin Trough and Warsaw Trough. Based on these results, six geothermal district heating (GeoDH) projects, in various stages of development, have been located. One of the most prospective areas for the wide range use of geothermal waters in the central part of the Polish Lowlands is the area of Mogilno-Łódź Trough (MLT). In our study, the site favorable for EGS system, located at MLT, north-east of Poznań, Poland was investigated. In this area, Lower Permian sandstones, claystones and mudstones representing Playa, Eolian and Fluvial facies associations being possible target EGS reservoirs were examined. In 2019, in the study area, the K-1 well was drilled as an oil and gas exploratory well. It identified a Zechstein salt pillow and provided valuable information on the geology and physical rock properties of Mesozoic and Permian strata. This enabled re-evaluation, reinterpretation and 3D modeling of vintage data combined with newly acquired data from K-1 well. The well, the deepest in the area, may be a reference in the further recognition of the axial part of MLT, not penetrated by drilling works. The K-1 well resulted in a unique data set for analysis of possible EGS utilization of the Rotliegend complex. The research comprises two variants of the structural and parametric (including temperature) 3D models. The model in variant one (SMV1) reflects regional variability based on a broad array of geophysical logs, including thermal logging from wells located within MLT, as well as in the marginal parts of surrounding

Mid-Polish Swell (MPS) and Fore-Sudetic Monocline (FSM). They were input for regional models of porosity, permeability, clay content and thermal parameters distribution. For this study, the local inset covering Kłecko Anticline was extracted from the regional model as SMV1 and then used for geothermal potential assessment. Unlike the previous regional considerations on geothermal prospectivity [1,2], the SMV1 model was obtained using 3D modeling workflows derived from the petroleum geology [3,4]. The modeling process results, supported by statistical analysis, indicate higher geothermal prospectivity than resulted from previous studies provided with the application of more traditional methods and/or archival data [1,2,5]. Structural framework of the model in variant two (SMV2) integrates results of the new 2D seismic interpretation and the results of the K-1. It reflects very complex tectonics of the Kłecko Anticline, hence it demanded even more advanced methods of modeling comprising the Structural Framework Modeling method. Parametric models included in SMV2 use regional trends of SMV1, as guiding models, but results of local modeling are strongly modified using interpretation of logs from the K-1. Both variants of models were used for further assessment of geothermal energetic potential (prospective resources) of the EGS reservoirs, comprising the Playa, Eolian and Fluvial complexes. Their comparison and statistical analysis indicate the importance of local structural and geothermal anomalies related to halo-tectonic structures and shows that the Kłecko Anticline could be the first EGS site in the Polish Lowlands, as the temperature in the most prospective Eolian complex is about 10% higher than regional expectation presented by SMV1 (160 °C vs. 150 °C), improving conditions of electric power generation.

2. Geological Setting

The investigated area is located within the Mogilno-Łódź Trough [6,7], a tectonic unit being the part of the West and Central European Paleozoic Platform (WCEPP) margin, the zone comprising terranes such as the Trans-European Suture Zone (TESZ) or Brunovistulicum (Figure 1B) [8,9]. This corresponds to the eastern extension of the Permian and Mesozoic system of epicontinental basins of Western and Central Europe—the Mid-Polish Trough (MPT) [10–14]. According to the newest research, the Permian-Mesozoic architecture of MPT inherited its foundations after the Ediacaran rifting phase of Rodinia, which resulted in lithosphere thinning [15,16]. The direct impulse for the MPT development was the rifting phase in the latest Carboniferous to Early Permian, which was coupled with intensive volcanic activity that was followed by post-rift thermal subsidence and the deposition of Lower Permian Rotliegend clastics and Zechstein marine deposits [17,18]. Thermal subsidence of the MPT lasted up to the Late Cretaceous, involving three main pulses in: (1) Zechstein to Olenekian; (2) Oxfordian to Kimmeridgian; and (3) the Early Cenomanian [18,19]. The final stage of the MPT evolution was Late Turonian through Paleocene compressional inversion [11–15,19,20]. The MPT's inversion was a widespread uplift typical for basins with thick salt sequences. Inversion and subsequent erosion created the present-day structural pattern of the Polish Lowlands, including the Fore-Sudetic Monocline, the Szczecin Trough, the Mogilno-Łódź-Miechów Trough, the Mid-Polish Swell (Anticlinorium) (MPS) and the North-Eastern Marginal Trough (Figure 1A) [6,7,21]. Regional subsidence patterns of the MPT locally were superimposed by salt movements that started in the Early Triassic [12,13,22,23], resulting in a complex system of salt structures in the central and NW segments of the Polish Lowlands [12,13,24]. The final stage of tectonic evolution of the Polish Lowlands involves Cenozoic Graben system development during the latest Eocene to Mid-Miocene times [11,14].

The MPT is underlain by 5–6 km thick complexes of Lower Paleozoic and Devonian-Carboniferous sediments [19]. Permian-Mesozoic sedimentary successions of the MPT are, in general, continuous from the Rotliegend up to the Upper Cretaceous (Maastrichtian) strata, reaching a thickness of 8 km in the area close to East European Craton (EEC) [25–28]. Deposits of the Rotliegend group are represented by volcanic and terrigenous series, divided into a number of formal lithostratigraphic or allostratigraphic units [29–35]. They can be correlated with those in the German part of the Southern Permian Basin [36]. However,

in petroleum exploration practice, terrigenous complexes of Permian in Poland are traditionally subdivided as non-reservoir Autunian and generally prospective Saxonian. The latter is represented by eolian and fluvial sandstones, playa mudstones and siltstones [35,37,38]. A maximum thickness of the Rotliegend continental clastic sediments in the MPT reaches 1400 m [39].

Rotliegend deposits are covered by a Zechstein marine—carbonate and evaporite—cyclic sequence. In the MPT, it is represented by four evaporitic cycles, known as the Werra (Z1), the Stassfurt (Z2), the Leine (Z3), and the Aller (Z4), and in westernmost Poland by the youngest cycle, the Ohre (Z5) [27,40,41]. Original depositional thickness of the Zechstein probably reached up to 1500–2000 m in the MPT axial zone [41], gradually pinching out towards the basin margins (Figure 1).

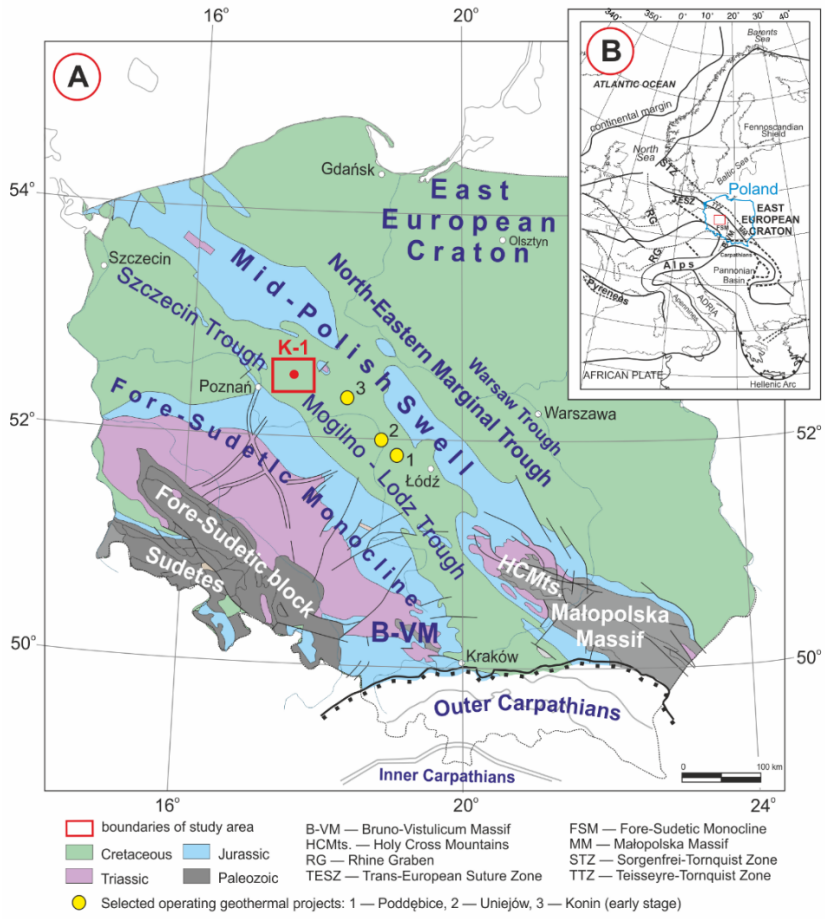

Figure 1. Regional geology of the central part of Polish Lowlands: (**A**) Cenozoic subcrop map [42]–simplified; (**B**) Europe scale tectonic setting of the area of interest, based on [43]–modified.

The internal part of the basin is, in general, dominated by salt facies, gradually replaced at margins by sulfate and clastic ones. As a result of intensive salt movements (Triassic to Paleocene), thickness of Zechstein in salt diapirs, in the Szczecin-Mogilno-Łódź Trough and the Mid-Polish Swell, locally reaches over 5000 m (Figure 2).

In the latest Permian to Anisian times, the evaporitic sabkha sedimentation of the uppermost Zechstein was replaced by continental—fluvial, lacustrine and playa deposits of the Buntsandstein Group, comprising three subgroups: Lower, Middle and Upper [44]. In regional mapping and petroleum exploration practice, deposits of the Lower Buntsandstein Group (LBS) and the Middle Buntsandstein Group (MBS), because of their continental provenance, are referred to as Lower Triassic. The LBS deposits are mainly fluvial to lacustrine [44] with marginal brackish intercalations [45,46]. The MBS is composed of alternations of thin-bedded sandstones, siltstones and claystones of playa and lacustrine

origin. The thickness of the Lower Triassic complex in the Polish Lowlands is considerable and locally exceeds 1500 m.

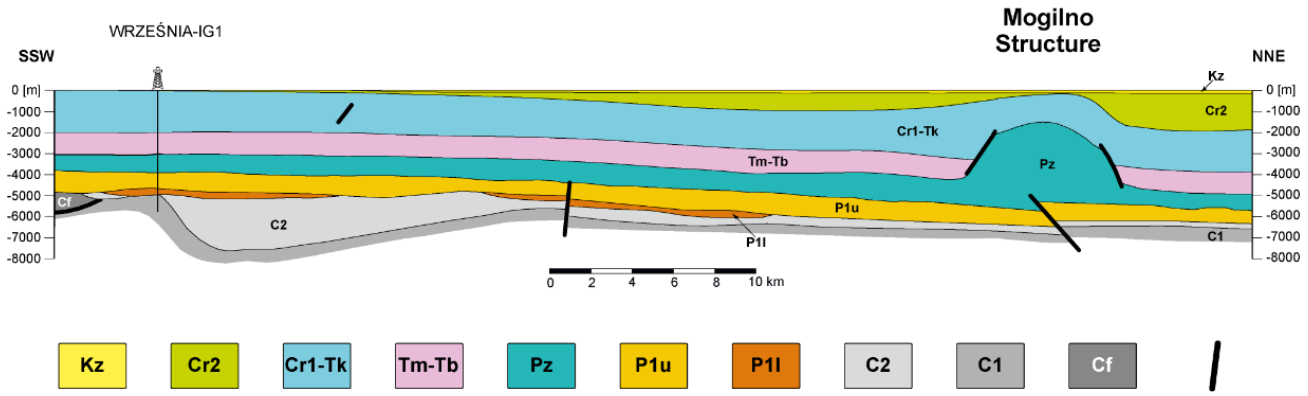

Figure 2. Geological cross-section through the study area (Kz—Cenozoic, Cr2—Upper Cretaceous, Cr1-Tk—Lower Cretaceous Upper Triassic (Keuper), Pz—Zechstein, P1u—Upper Rotliegend, P1l—Lower Rotliegend, C2—Upper Carboniferous of the Hercynian Foredeep, C1—Lower Carboniferous of the Hercynian Foredeep, Cf—undivided folded Carboniferous of the Hercynian Orogenic Belt, bold line expresses the major faults).

The Middle Triassic in the MPT is represented by marine deposits. The succession starts with the Upper Buntsandstein Group's strata (equivalent of the Röt Formation) represented by calcareous Rötdolomit and Rötkalk of southern Poland. It is also represented by a large brackish-water lagoon with predominantly fine-grained red clastics of a semi-closed evaporitic basin. They were gradually replaced by shallow sea carbonate sedimentation and the marine and hypersaline carbonates known as Muschelkalk [47].

Upper Triassic of the MPT contains shale dominated deposits of Ladinian through Rhaetian succession that is an equivalent of Keuper Group (KG), which is divided into three subgroups. The Lower Keuper Subgroup (LKS) strata are represented predominantly by gray clastic deposits that were accumulated in various continental environments. The Middle Keuper Subgroup (MKS) was deposited mainly in ephemeral-lake and fluvial systems. The section of the MKS begins with evaporites and shales of the Lower Gipskeuper. They are covered by the Schliff Sandstein (Stuttgart Formation) strata, which is dominated by fluvial plains to fluviodeltaic mudstones and sandstones [26,48]. The next complex of the MKS is Upper Gipskeuper strata (Weser Formation), that are represented by evaporates of salina, sabkha or playa mudflats environments. The uppermost part of the MKS belongs to the Playa Arnstadt Formation (Steinberger Keuper). The uppermost Triassic (Rhaetian) deposits belong to the Upper Keuper Subgroup (UKS). They are the youngest part of the Triassic. In the MPT the UKS consists of non-marine fluvial and lacustrine deposits [47,48].

The Lower Jurassic (Hettangian to Toarcian) succession, starting from coarse-grained clastic sediments, predominantly consists of shallow-marine, brackish to fluviodeltaic provenance. The Lower Jurassic rocks are represented by the Kamienna Group, which is subdivided into up to 12 formations [49]. The Lower Jurassic strata reach thicknesses of up to 1300 m in the axial part of the MPT [50,51].

The Middle Jurassic interval is represented by deposits of four stages—the Aalenian, Bajocian, Bathonian and Callovian. The MPT was partly isolated from the basins of western Europe during Aalenian and Bajocian times [50,52]. Deposition in the MPT is characterized by marine clastic sedimentation in the uppermost part (Callovian) replaced by marine carbonates.

During the Late Jurassic, deposition was initially restricted to the axial parts of the MPT, and it was dominated in the north by a clastic sedimentation (>800 m thick in the Pomeranian Basin). To the south a transition to carbonate-dominated, >1400 m thick, shelf sedimentation was observed [53]. Starting in early Oxfordian times, deposition of marly

mudstones, carbonate-cemented glauconitic sandstones and sponge-rich lime-mudstones (Łyna Formation) was observed. Northwards it is interbedded with the Chociwel Formation's sandstones as well as limestones of the Brda Formation in the central, western and northern part of the Polish Lowlands [54,55]. In the central part of the basin massive limestones, partially silicified, sponge-rich or dolomitized are dominant deposits. Within the upper Oxfordian strata, coral bioherms (Coral Formation) are locally developed. Late Oxfordian–early Kimmeridgian strata were deposited in carbonate-shelf environments, replaced in Tithonian times by a restricted brackish basin, where Middle Tithonian limestones with shell beds gradually pass into anhydrites, dolomites and gypsum, ostracod-rich limestones, marls and sandstones of the upper Tithonian.

Cretaceous deposits survived mostly in the post inversion troughs (Figure 1A). The Lower Cretaceous section in the Mogilno-Łódź Trough (MLT) is represented by the sandy deposits of Middle Albian, Barremian, Hauterivian, and Valanginian. The best reservoir interval comprises the Mogilno Formation (Middle Albian through Barremian) represented by Pagórki Mb. (sandstones), Gopło Mb. (mudstones and sandstones) and Kruszwica Mb. (sandstones) [56]. In the Polish Basin, Upper Cretaceous deposits represent six individual transgressive-regressive cycles [20,56,57]. Generally, they were laid down in an open basin and shelf environments. In the MLT they are represented by associations of carbonate-siliceous, carbonate and marly lithofacies, often containing thick complexes of gaises and opokas [20].

Lower Jurassic to Cretaceous successions in NW and SE Poland were subsequently removed by Upper Cretaceous–Paleocene inversion of the MPT to the Mid-Polish Swell (Figure 1A).

3. Geothermal Setting

Regional geothermal conditions of the Polish Lowlands have been a subject of research since the end of the 1980s, starting from the early works of Sokołowski [58] through Górecki's series of geothermal atlases [1,2,59–62], up to an investigation on Enhanced Geothermal Systems [5,63]. These works were followed by further regional and semi-regional projects conducted in 2020 by the AGH University of Science and Technology. These projects introduced the new quantitative approach based on 3D static models [64–66] that applied modified workflows elaborated for petroleum exploration as well as Carbon Capture and Storage (CCS) purposes [4,67].

In the Polish Lowlands, most geothermal aquifers are commonly represented by siliciclastic rocks, mainly sandstones, in which the geothermal potential, apart from temperature, is controlled by petrophysical rock properties, mainly intergranular effective porosity and intrinsic permeability. These parameters strongly depend not only on sedimentology and petrography (chemical composition of matrix) but are strongly influenced by a chemical composition of formation waters and the temperature. Other factors that affected reservoir quality were also compaction and inversion episodes related to tectonic evolution. All geothermal aquifers of the Polish Lowlands can be classified as conduction-dominated geothermal plays. Regarding the considerable similarity of the geology between the Polish and German parts of the Southern Permian Basin, play classifications [68] derived in Germany can be applied. It allows to identify within the Polish Lowlands two types of geothermal plays—Intracratonic Basin (CD1 Plays) and Crystalline Rock Basement (CD3 Plays in Figure 3). In this case, CD3 Plays type is represented by sedimentary EGS plays [68–70]. The CD1 Plays in Poland represent commercially developed reservoirs of Lower Jurassic and Lower Cretaceous. CD3 Plays are, in Poland, only a subject of theoretical considerations, which allowed identification, in the Kuiavian segment of the Mid-Polish Swell, a possible sedimentary EGS play, in low porosity and low permeability sedimentary rocks of Lower and Middle Buntsandstein [63] as well as in volcanic covers of Autunian in the western part of the Fore-Sudetic Monocline [5]. In these works, Rotliegend deposits were also qualified as possibly favorable for EGS development, but they have not yet been recognized in detail.

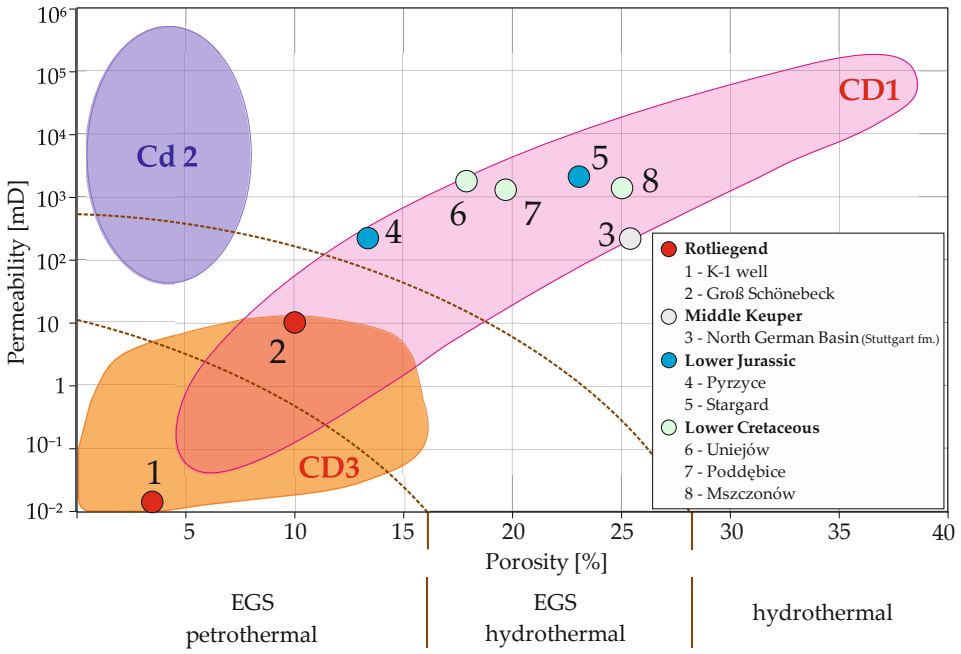

Figure 3. Compilation of operational geothermal reservoirs in Poland, their host rock formations, porosity, and permeability on the basis of the geothermal play types (explanations: CD1—Intracratonic Basin Play type, CD2—Foreland Basin Play type, CD3—Crystalline Basement Play type, based on [70], simplified).

Deep-seated phenomena, including continental crust thickness, massive volcanism or plutonism affect the terrestrial heat flow density (HF) and geothermal gradient distribution. In general, the Polish Lowlands are characterized by a low-to-moderate HF. According to different research, HF values range from ca. 30 to 110 mW m^{-2} [71–73] and from ca. 30 to 90 mW m^{-2} [74–76] – more likely. Consequently, an average geothermal gradient varies from 1 to ca. 3.8 °C 100 m^{-1} [77,78].

The Polish Lowlands can be divided into two basic thermal provinces: the relatively cold Precambrian EEC and the relatively warm WCEPP (Figure 1). Usually, HF in the EEC area is below 55 mW m^{-2}, whereas in WCEPP it is distinctly higher and more diversified, reaching from <55 to >80 mW m^{-2}. The highest heat flow values have been noticed from northwestern Poland in the area of the Fore-Sudetic Monocline, within an approximately 50–70 km wide belt. This zone corresponds to the trend of continental crust thinning [76,79]. The zone of the highest HF corresponds to the location of the thick (up to 1000 m) volcanic cover of Autunian, but their quantitative relationships have not yet been recognized.

In the area of the MLT two operating GeoDH plants are located in the towns of Uniejów and Poddębice. Both of them use geothermal waters from a Lower Cretaceous aquifer [61,62,65,66,80]. Detailed operating parameters of the heat plant in the Mogilno-Łódź Basin are presented in Table 1. The most recent geothermal project, located close to the study area, is the Konin GT-1 geothermal well, drilled in 2015 to the total depth of 2660 m. During the testing, the water temperature at the well-head reached 92 °C, which is the highest value reported from Poland. The temperature of thermal brines at the bottom of the Lower Jurassic reservoir reaches 97.5 °C. The well productivity has been determined as 114 m^3 h^{-1} (2736 m^3 day^{-1}). All geothermal projects completed up to now have been focused on reserves accumulated in Mesozoic hydrothermal aquifers. The geothermal potential of Paleozoic formations has still not been unlocked.

Table 1. The main operating parameters of the geothermal installations in Mogilno-Łódź Trough.

Location (City)	Aquifer	Well-Head Temperature	Admissible Water Productivity	Water Mineralization	Installed Geothermal Capacity	Total Installed Capacity (Geothermal Plus Peak Load)	Annual Heat Production
		°C	$m^3\ h^{-1}$	$g\ dm^{-3}$	MW_t	MW_t	$TJ\ a^{-1}$
Poddębice	Lower Cretaceous	71	252	0.4	10.0	10.0	63
Uniejów		68	120	6-8	3.4	7.4	9

Other minor but also important factors deciding on the EGS location are:

- Resistance to water saturation, especially resistivity to swelling, generally going along with the low clay content.
- Susceptibility to massive fracturing.
- Lack or very weak inflow of groundwater into EGS system.
- Maximum allowable reservoir temperature drawdown during the operation—10%.
- Low flow losses in the EGS system—below 10% of injection flow.

Recognized analogs for Paleozoic geothermal prospects within the Polish Permian Basin can be found in the Northeastern German Basin. Both basins combined together form one huge Pan European structure called the Central European Basin, where a significant geothermal potential is being reported [81]. The best-known geothermal installations located in the central-north part of Germany are: Groß Schönebeck (with 150 °C at 3830–4250 m b.g.l.), with Rotliegend tight sandstone and andesites [82,83], Neustadt-Glewe (with 98 °C at 2195–2300 m b.g.l., and productivity of 100 $m^3\ h^{-1}$) and Waren (Müritz) (with 63 °C at 1540 m b.g.l., and productivity of 60 $m^3\ h^{-1}$) within the Rhaetian sandstone reservoir [84].

The studies on EGS geothermal plays, including the Polish experience and specific geological conditions, allowed to elaborate the criteria for development of a commercial geothermal plant in a low permeability and porosity reservoir [5,69,85–89]. The K-1 well is located close to the axis of the western part of the Mogilno-Łódź Trough, on the northern slope of the significant positive HF anomaly of the Fore-Sudetic Monocline. According to legacy data, HF value at K-1 location varies about 85 $mW\ m^{-2}$ [71,72,74–76], while the estimated temperature at the top of the Rotliegend was approximated as about 139 °C, at a depth of ~4300 m b.s.l., and thermal gradient ca. 2.9 °C $100\ m^{-1}$. So far, rather sedimentary Lower Triassic deposits were suggested as more EGS system ready than the Rotliegend one in the Polish Lowland [5,63]. However, the above comparison to the German Basin and the inspection of basic requirements, which should be satisfied to locate the EGS plant (Table 2), speaks for possible increased prospects for K-1 region.

Table 2. List of criteria and parameters conditioning preliminary selection of geological structure for EGS system based on a literature review.

Parameter	Minimum Value	Data Source
	Major Criteria	
Reservoir depth	5–6 km	[90,91]
	4–6 km	[5]
Reservoir thickness	≥200 m	[5]
	≥300 m	[92]
Reservoir rock temperature	90 °C (minimum temperature for electric power production)	[91]
	>100 °C (enough for heat production for GEODH or moderate for binary cycle electricity production)	[69,86]
	>150 °C (effective electricity production)	[69,85]
Initial permeability	The lower the better (<3 mD)	[93]

Table 2. *Cont.*

Parameter	Minimum Value	Data Source
	Major Criteria	
Effective porosity of the rock mass	The lower the better (<3%)	[5]
Caprock thickness	>20 m	according to CCS requirements [94]
	Minor criteria	
Thermo-physical parameters of the reservoir rocks	High thermal conductivity and high specific heat of reservoir rock	[69,85,86]
Circulation flow rate	30 l s^{-1} (ca. 108 m^3 h^{-1})	[85]
	50–75 kg s^{-1} (ca. 180–270 m^3 h^{-1})	[95]
	50–100 kg s^{-1} (ca. 180–360 m^3 h^{-1})	[96,97]
	50–100 l s^{-1} (ca. 180–360 m^3 h^{-1})	[98,99]
Rock volume accessed	$>2 \cdot 10^8$ m^3 = 0.2 km^3	[100,101]
Effective heat transfer area	$>2 \cdot 10^6$ m^2	[95]

4. Materials and Methods

The case presented in this paper is an excellent example of quantitative assessment of regional geothermal conditions and potential predictions under specific, locally anomalous geological conditions, disclosed with results of the new deep well. Such a case enforces application of a variety of methods, starting from a sample-scale, through a well-scale, up to a basin-scale analysis. The K-1 well completion has given a new look into the geological and thermal conditions of the central part of the Mogilno-Łódź Trough. Logging and coring enabled advanced core-based analysis.

4.1. Sample Based Interpretations

The latter were completed on samples of Rotliegend rocks, the only cored interval in the well. To calibrate thermal analysis, thermal conductivity (TC) measurements were conducted with the steady-state method by determining the heat flow through the sample using a FOX50–190 LaserComp apparatus. The tests were carried out on 5 samples in the shape of 2 cm thick tubes and 5 cm in diameter. The measurements were completed on dry samples in the temperature range 152–168 °C, corresponding to reservoir conditions. The results of the measurements carried out are presented in Table 3.

Table 3. Thermal conductivity measurements for Rotliegend rock samples from K-1 well.

Sample Code	Rock Sample Lithology	Sample Depth m b.g.l.	Measurement Temperature °C	Thermal Conductivity W $(m\ K)^{-1}$
S1	mudstone	4585.15	152	1.125
S2	sandstone	4687.12	154	2.906
S3	sandstone	4832.60	157	2.821
S4	mudstone	5061.38	164	2.379
S5	volcanites	5180.35	168	2.134

The parameter was examined on 5 samples of Rotliegend mudstones and shales, more for qualitative than quantitative reasons. The main goal of that analysis performed was checking whether the rocks are stable enough to perform hydrofracking. The LST tests showed that the examined rocks slightly swell under the influence of FFS under high pressure (1500–2000 psi) and high temperature (160–170 °C). The observed swelling values vary in the range of 4.6–8%.

4.2. Log-Based Interpretations

Log-based interpretations are of crucial importance in the process of spatial geomodeling. Well logs enable both stratigraphic interpretation and quantitative description of petrophysical, lithological and physical parameters of depositional sequences. In the study, results of industrial volumetric interpretation of basic rock components (quartz, calcite, dolomite, anhydrite, halite, clay minerals) as well as water and gas saturation from many wells were used (Figure 4).

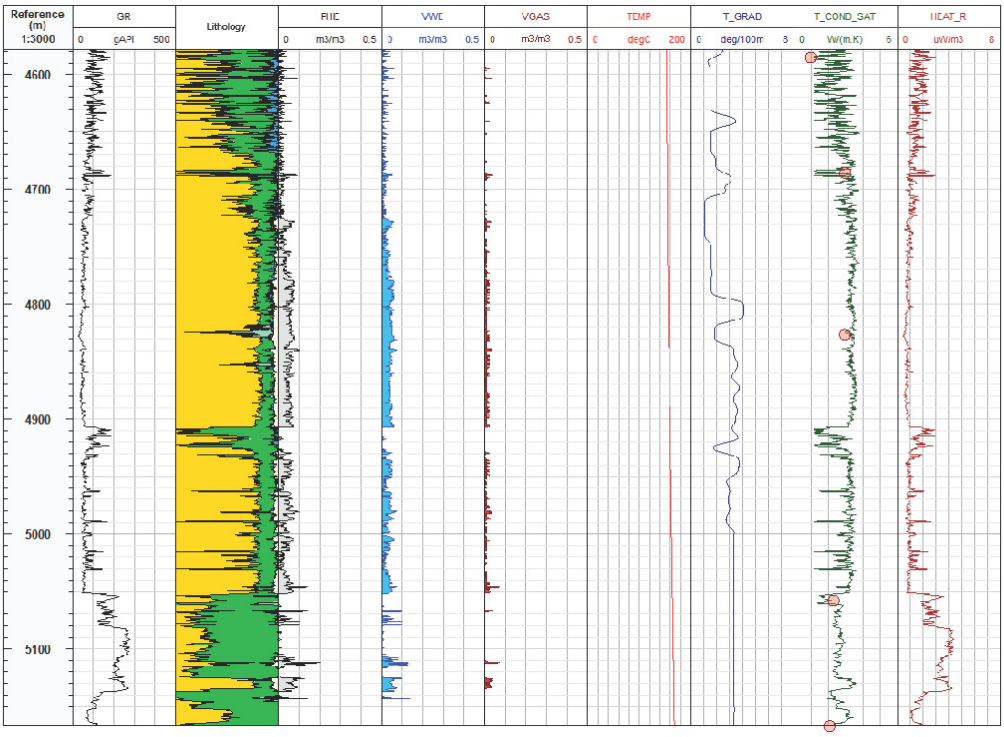

Figure 4. Volumetric interpretation of basic rock components and thermal parameters for the interval 4580–5170 m in K-1 well (lithology: yellow—sandstones, green—claystones, light blue—limestones, dark blue—dolomites; GR—natural gamma ray, PHIE—effective porosity, VWE—effective water fraction, VGAS—gas fraction, TEMP—temperature, T_GRAD—thermal gradient, T_COND_SAT—thermal conductivity for saturated conditions, HEAT_R—radiogenic heat; red circles on the thermal conductivity track—calibration points).

The very recent completion of the K-1 well allowed for reliable estimation of the thermal conductivity logs, using commonly described methods [102–107], that in the Rotliegend interval were calibrated with laboratory measurements. Available data allowed to apply a mixing law model to calculate bulk TC for the whole drilled section using textbook TC values (Figure 5).

Following the experience of previous authors [108–110] as well as Tatar et al. [111] analysis, the geometric mean model, originally introduced by Lichtenecker [112], was used to calculate the saturated bulk TC. Thermal conductivity of selected rock's components, and reservoir media used for the calculations performed in the study is shown in Figure 5. Because of lack of appropriate data, the correction for pressure was not computed.

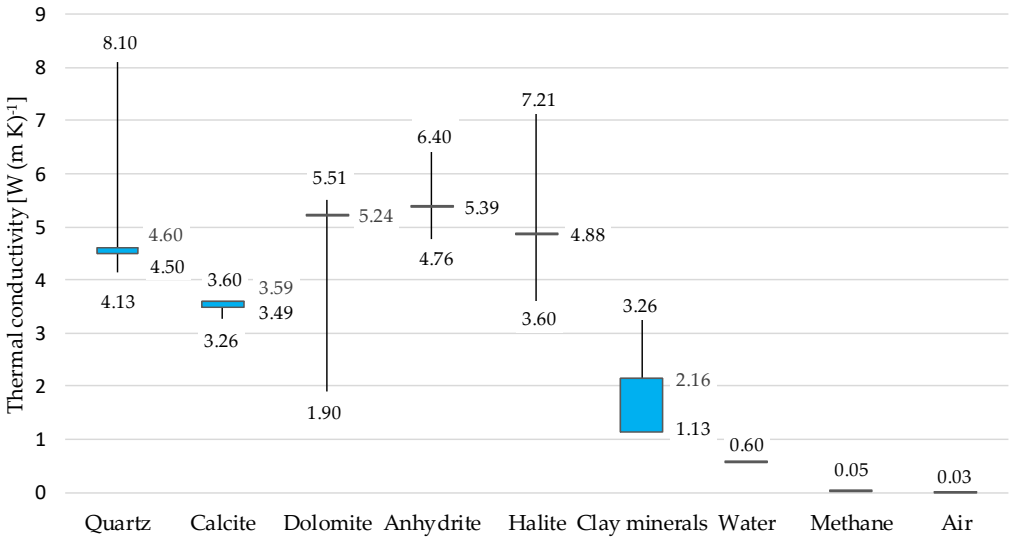

Figure 5. Open-high-low-close chart of thermal conductivity of selected rocks and reservoir media according to [77,107,110,111,113–118] (OC—blue bars express thermal conductivity values of particular rocks and media used for the calculations performed in the study).

In the K-1 well the thermal logging was performed in the perturbed conditions in several runs. The logs were combined into a composite, standardized to the quasi-equilibrium conditions with the application of method described by Kudrewicz [119], and calibrated by DST results. The standardized composite log was then used for determination of the thermal gradient log, which was computed by a differentiation of the thermal log. The characterization of thermal parameters was extended by computation of the heat flow (HF), as well as radiogenic heat (RH) logs. In the case of conductive flow, the basis for calculation of heat flow value is the depth-related rate of temperature changes observed in the wells analyzed together with thermal conductivity. The mathematical expression describing the relationships between the above-mentioned values is the Fourier's [120,121] Equation:

$$Q = -k \cdot \nabla T \quad (1)$$

where:

Q—heat flow (W m^{-2});
k—thermal conductivity (W (m K)$^{-1}$);
∇T—thermal gradient (°C m^{-1}).

RH log reflects radiogenic heat produced by the rocks. In the described case, it was assessed in K-1 well, based on the Bücker and Rybach [122] formula that is related to natural gamma ray directly:

$$A = 0.0158 \cdot (GR - 0.8) \quad (2)$$

where:

A—radiogenic heat (μW m^{-3});
GR—natural gamma ray (API).

5. Spatial Interpretation

Contemporary 3D static geomodels created for geothermal or petroleum exploration purposes tend to be multiscale solutions that can be used in resolving regional to local scale exploration problems [4,37,103,123–125]. Models can be invaluable for integrating, understanding and supporting petroleum and geothermal field decisions [3,126,127].

In this paper, spatial modeling results are presented in two variants. The first one, referred to as the structural model in the variant 1 (SMV1), is a regional solution based on public data [1,2,28] and own materials. It was generated using simplified structural-

parametric modeling workflows, suited to the large spatial extent of the model, which covers a couple of structural units (Figures 1 and 4). This model, although very large in spatial extent, needs to support moderate to high horizontal and vertical resolution, which assure satisfying fitting of the parametric model and the input log-data. Such solutions are delivered by Petrel's tools—Simple Grid [SG] and especially Corner Point Gridding [CPG] methods. This manner of structural modeling is known as pillar gridding or surface-based approach. The CPG firstly models fault as pillars and horizons as smooth planes, and later creates geological layers by following defined topological relationships. The CPG is represented by a set of hexahedral blocks with eight nodes and 12 edges. In the case of SG, where faults are replaced by acute variability of the input surfaces, the 3D model is composed of regular hexahedrons.

Prior completion of the K-1 well, prediction of the structural, facies and petrophysical variability in this region was based on regional trends. Only 13 wells deeper than 500 m, but not reaching the top Middle Buntsandstein, and results of the regional seismic lines ZRG00897 and ZRG00997 interpretation [39] (Figure 6) were located within structural model variant 1 (SMV1). Well logs from these wells do not contain data suitable for thermal or petrophysical analysis. Such a situation resulted in the necessity of regional trend extrapolation at the K-1 well vicinity. To gain this objective, the authors primarily build a temporary structural model covering the MLT, the northern part of FSM and the southern part of the MPS. The input data set used for construction of structural model version 1 were regional structural maps of particular stages in interval base Cenozoic through top Devonian, prepared and systematically updated by an AGH University of Science and Technology team [1,2,28,64]. Then, this geometrical framework was used to prepare a regional scale parametric model (SMV1). The large area of the regional framework covers quite a considerable quantity of input data (Table 4).

Table 4. Input data for parametric modeling in variant 1 (in structural framework SMV1) and variant 2 (in structural framework SMV2).

Model	Permeability PERM	Porosity PHI	Shale Volume VSH	Bulk Density RHOB	Temperature °C
SMV1	98	107	84	37	55
SMV2	99	108	85	38	56

Most of the input data have been collected and/or interpreted during preparation of geothermal atlases [1,2], and regional analysis of hydrocarbon potential of the Rotliegend in Poland [37]. A very small portion of well data have been acquired for geothermal exploration. Most of the deep wells were designed for hydrocarbon exploration, and they are rarely located to the north of the FSM. The closest deep wells that have reached the top of Rotliegend are: Września IG-1 (17.5 km from SMV1 border), Środa IG-2 (17.6 km), Objezierze IG-1 (26.5 km), G-2 (34.0 km), Czeszewo IG-1 (39.0 km), Bygoszcz IG-1 (51.0 km), Piła IG-1 (61.3 km), and B-1 (66.2 km). They are located in the area of the MLT, MPS or FSM, and they have been used in the modeling of temperature, VSH and PHI. Other, not distant, wells used in the modeling of shallower complexes were, e.g., Swarzędz IGH-1 (17.5 km), Wągrowiec IG-1 (10.0 km), and Cykowo IG-1 (45.9 km).

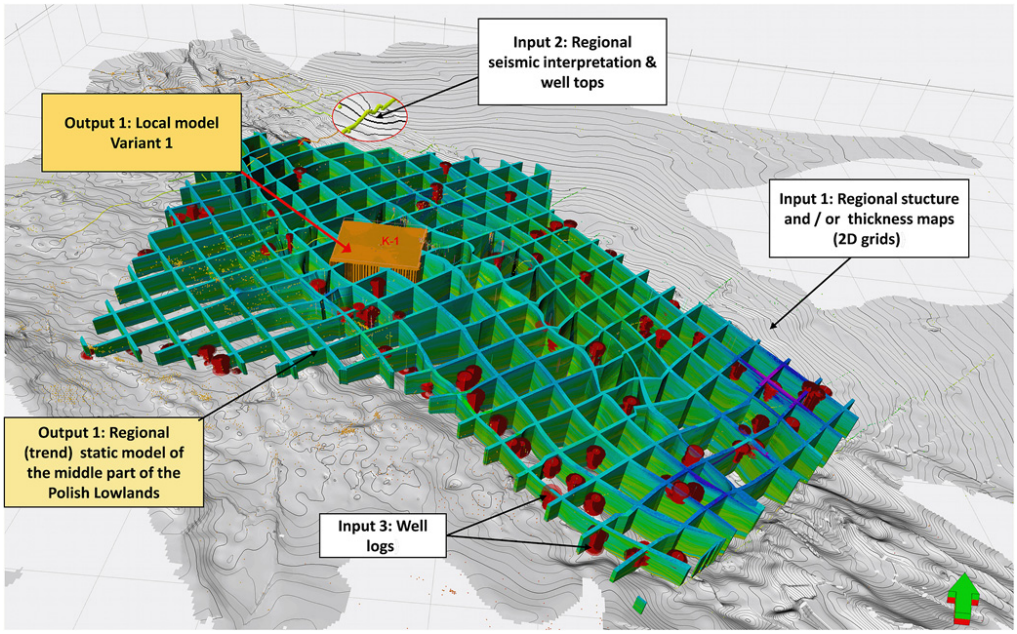

Figure 6. An example of input data applied for generation the first variant of the structural model (SMV1).

Using that kind of framework, working regional parametric models in the first variant (SMV1) of temperature (TEMP), porosity (PHI), shale volume (VSH) and bulk density (RHOB) were constructed. The model representing the second variant (SMV2) reflects local modifications that were introduced as a result of K-1 well completion, and interpretation of the new seismic data acquired in this area (Figure 7).

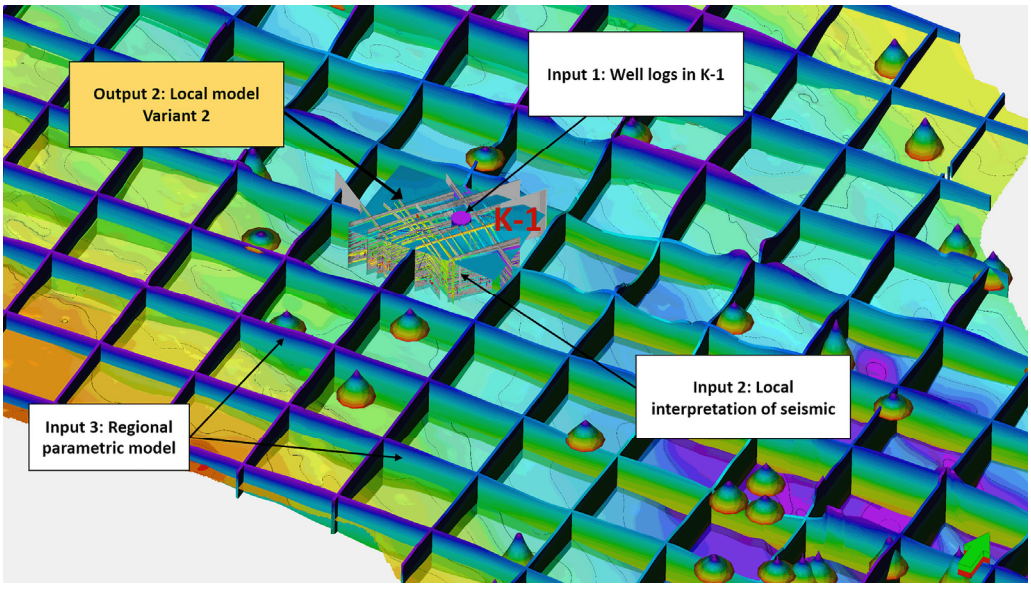

Figure 7. The structural and parametric model in variant SMV2.

This modeling disclosed very complex tectonic settings of the area—different for pre-Zechstein, Zechstein and post-Permian strata. Such complex tectonics excludes use of the CPG method in detailed structural modeling of the area. Petrel's tool dedicated to solving geometry of such complex regions is called structural framework (SF) and uses the Volume Based method. Geological layers are modeled directly by using an unstructured tetrahedral mesh, which is internally constrained by faults [4,128,129]. The second variant of the

structural model, structural model in variant 2 (SMV2), of the K-1 region was constructed in the local scale with application of the SF method and SF to CPG conversion. Parametric models of SMV1 although locally fitted to K-1 were externally controlled (trended) by regional parametric models, using multiscale modeling workflows [4,67,125,130].

6. Methodology of the Preliminary EGS Potential Assessment

Methodology of the EGS potential assessment is a development of conventional geothermal reserves assessment. It relies mostly on assessment of volume mass of rocks and accompanying fluids (heat in place—HIP), along with the estimation of temperature and other parameters. The volumetric method is often used to provide estimates of the probable electrical generation capacity of a geothermal system.

Apart from the assessment of theoretical potential (relating to annual mean ambient temperature—T_0), most of the research was focused on issues concerning the assessment of so-called technical and economic potential. Technical potential includes, among others, the estimation of the recoverable fraction (recovery factor—R) of reserves suitable for the utilization from a technical point of view. The assessment of technical reserves, unlike theoretical ones, requires among others determination of the heat utilization technology, including heat and/or power production. Moreover, the recovery factor also depends on efficiency of the thermodynamic cycle, the minimum operating temperature, production temperature and the output, re-injection temperature and others. A simplified division of the geothermal potential classes is shown in Figure 8.

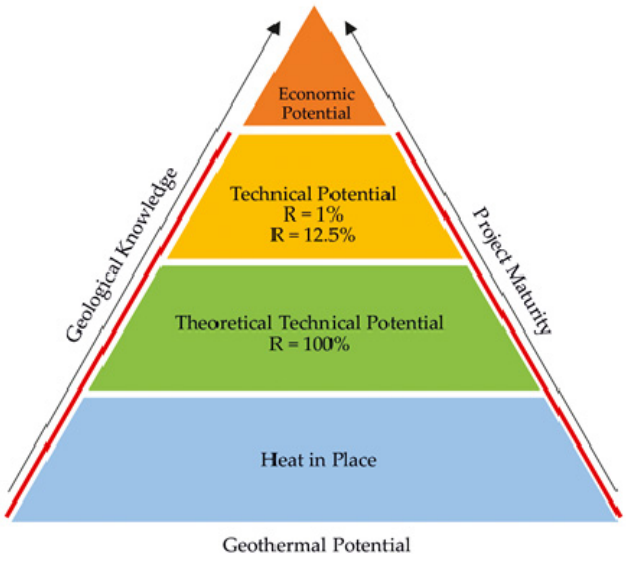

Figure 8. One-dimensional division of the geothermal potential classes—from theoretical to realistic—based on [131,132], modified.

The principles of the volumetric method of HDR/EGS resource and reserves assessment have been broadly discussed and applied for decades [63,91,132–138]. The methodology for the evaluation and/or reporting of EGS resources and reserves, taking into account environmental and economic considerations, has been the subject of many projects and research work. The best-known practices and approaches are presented in, e.g.,

- Massachusetts Institute of Technology (MIT) Interdisciplinary Panel [69];
- Canadian Geothermal Code for Public Reporting, by the CGC Committee [139];
- A Protocol for Estimating and Mapping Global EGS Potential [135];
- New Geothermal Terms and Definitions—the Geothermal Energy Association [140];
- Resource Assessment Protocol for GEO-ELEC [141];
- United Nations Framework Classification for Fossil Energy and Mineral Reserves and Resources 2009 (UNFC-2009) [142].

For this study, the methodology and approach developed under the GEO-ELEC project [132] were employed. Because this is the first attempt at EGS potential evaluation for Kłecko Anticline, an economic issue was not analyzed. This study is solely focused on the theoretical and technical potential according to the definitions given by [97,132,135].

6.1. Theoretical Potential of EGS

The theoretical potential (Eth) of the K-1 structure was calculated according to the Rybach's [97] definition and Equation (3).

Heat in place (*HIP*) is defined as total heat stored in rock mass volume, including rock matrix, formation fluids, and reservoir temperature. In EGS systems, due to assumed low effective porosity, fluid heat content is negligible:

$$HIP = V \cdot \rho_{rock} \cdot c_{rock} \cdot \left(T_{prod} - T_0\right) \cdot 10^{-15} \quad (3)$$

where:

HIP—heat in place (PJ);
V—reservoir volume (m^3);
ρ_{rock}—rock density (kg m^{-3});
c_{rock}—specific heat of reservoir rock (J $(kg \cdot K)^{-1}$);
T_{prod}—reservoir temperature at the midpoint (°C);
T_0—annual mean ambient air temperature (°C), T_0 = 8 °C, according to the Institute of Meteorology and Water Management (IMGW) [143].

The resulting HIP can be used to determine the theoretical potential for geothermal energy production considering realistic recovery factors and efficiency of standard geothermal power plants (Organic Rankine and Kalina Cycle).

Theoretical capacity (*TC*) is calculated as the heat in place multiplied by a conversion factor which depends on the mode of utilization. Theoretical capacity (Equations (4) and (5)) takes into account that energy cannot be utilized until the surface temperature (T_0). A return temperature (T_r), according to Williams et al. [91] and Beardsmore et al. [135], equal the cut-off temperature for the electricity production. For the study location T_0 = 8 °C [143], thus $T_r = T_0$ + 80 °C = 88 °C.

$$TC = HIP_e \cdot \eta_{th} \quad (4)$$

where:

TC—theoretical capacity (PJ);
HIP_e—effective heat in place (J);
η_{th}—cycle thermal efficiency for power conversion (–).

Effective heat in place (HIP_e) can be expressed by the following Equation (5) [132,135]:

$$HIP_e = V \cdot \rho_{rock} \cdot c_{rock} \cdot \left(T_{prod} - T_r\right) \cdot 10^{-15} \quad (5)$$

where:

HIP_e—effective heat in place (PJ);
V—reservoir volume (m^3);
ρ_{rock}—rock density (kg m^{-3});
c_{rock}—specific heat of reservoir rock (J $(kg \cdot K)^{-1}$);
T_{prod}—reservoir temperature at the midpoint (°C);
T_r—the cut-off production temperature for the electricity, equal to the temperature to which the crust can theoretically be reduced through the utilization of geothermal heat (assumed T_r = 88 °C);
(10^{-15})—conversion factor from J to PJ.

According to Beardsmore et al. [135], cycle thermal efficiency is plant-dependent, even for the same inlet fluid temperature. The design and arrangement of specific plant

components may include a trade-off between cost and efficiency. Cycle thermal efficiency, η_{th}, is a function of reservoir temperature and can be expressed by Tester et al.'s [69] formula, so since T_{prod} denotes the average reservoir temperature, η_{th} can be expressed with the following formula (Equation (6)):

$$\eta_{th} = 0.00052 \cdot T_{prod} + 0.032 \quad (6)$$

where:

η_{th}—cycle thermal efficiency for power conversion (–);
T_{prod}—reservoir temperature at the midpoint (°C).

6.2. Technical Potential of EGS

Technical potential denotes the expected recoverable geothermal energy (MW) [91,132]. The technical potential (*TP*) assumes that the reserves will be utilized for a period of 30 years (life span of power generation equals to 9.46 10^8 s). The conversion from theoretical capacity (*TC*) to technical potential (*TP*) is therefore Equation (7):

$$TP = 1.057 \cdot TC \cdot R \quad (7)$$

where:

TP—technical potential (MW_e km^{-2});
TC—theoretical capacity (PJ km^{-2});
R—recovery factor (0–1);
1.057—conversion factor from PJ to MW, considering 30-year life span.

Recovery factor (*R*) is the portion of heat that can ultimately be recovered from a volume of rock. The formula of recovery factor determination for the purpose of power production with EGS was the subject of in-depth studies [69,97,131,133,136]. All the above indicates that (*R*) depends on many theoretical assumptions, including reservoir, technical and environmental issues such as fractured volume of rock, permeability, and rock temperature, which are not possible to quantify at the early stage of the project like that currently being studied.

7. Results and Discussion

Analytical and modeling works completed for K-1 derived data provided for this study resulted in several types of products: calibration data, input data for modeling, complex geological interpretation, and potential assessment. The thermal conductivity measured by the FOX50–190 apparatus provided values of 2.821–2.906 W (m K)$^{-1}$ for sandstones, 1.125–2.379 W (m K)$^{-1}$ for claystones and 2.134 W (m K)$^{-1}$ for volcanic rocks (Figure 4). Based on methods described in previous sections, thermal gradient, thermal conductivity, and radiogenic heat production logs for the entire drilled interval were calculated, which allowed for the heat flux estimation.

The thermal gradient, determined for the entire drilled interval, varies along the well axis from 0.89 to 7.31 °C 100 m^{-1} with an average value of 2.9 °C 100 m^{-1}. The TC value varies from 0.95 W (m K)$^{-1}$ (claystone) to 5.52 W (m K)$^{-1}$ (evaporates). Radiogenic heat production varies from 0.16 to 7.07 μW m^{-3}. Heat flow density was assessed as 83.85 mW m^{-2}, with a negligible share of radiogenic heat at a level of 1.13%. Variability of these parameters for the Rotliegend interval is illustrated in Figure 4 and varies: thermal gradient from 1.07 to 4.10 °C 100 m^{-1}, thermal conductivity from 1.13 to 3.79 W (m K)$^{-1}$, and radiogenic heat from 0.45 to 4.39 μW m^{-3}.

These results together with remaining local and regional data were also used in the process of the creation of two variants of models differing with input data sets and local precision. The first group of spatial modeling results were structural models in two variants. The structural model in variant one (SMV1) was based on traditional, regional interpretation of the Mogilno-Łódź Trough's geological settings. They are rooted in assumptions and

results presented by, e.g., geothermal atlases of the Polish Lowlands [1,2], early research on the EGS viability in the area [5,63], or preliminary 3D models.

The regional structural solution presented as SMV1 is more sophisticated than the above-mentioned input maps, as it is based on more detailed mathematical models utilizing a new set of structural maps fitted locally to the recent version of stratigraphy in wells collected within the Central Geological Database—the part of the National Geological Archives (NGA), governed by The Polish Geological Institute—National Research Institute (PGI-NRI), as well as some minor stratigraphic reinterpretations, introduced by the authors, due to well log correlations within the area of the Kłecko Salt Anticline. Local adjustment involved 13 wells deeper than 500 m, and results of the regional seismic lines ZRG00897 and ZRG00997 interpretation (Figure 7). According to this interpretation, the Kłecko Anticline is a broad, NE-SW oriented fold (brachyanticline), developed over the Zechstein salt pillow, in the Mesozoic strata. It is cut along its axis by a normal fault extending from the Zechstein top up to the Cenozoic base. Its geometry is weakly controlled by seismic data, hence in the SMV1 the fault is interpreted as a vertical one. In the model, slopes of the structure are convex in shape, suggesting genetic similarity to the one proposed by Krzywiec [23] for the Szubin Anticline. The shape of the anticline and specific development of a stratigraphic column in the Kłecko-Geo 1 well, where a hiatus within Jurassic deposits is observed, led the authors to the assumption of the pillow's synsedimentary growth in the Late Triassic through Jurassic times, resulting in a temporary lack of deposition and/or erosion at the structure top.

In the SMV1, sub-Zechstein geometry was restored in accordance with the results of the regional petroleum system of the Rotliegend in the Polish Lowlands [37,144]. According to it, Rotliegend successions are represented by ~50 m of playa deposits, which rest on ~300 m of eolian sandstones, and ~250 m of fluvial-alluvial deposits, that in turn were lied down on the Late Carboniferous strata, that represent Variscian foredeep. According to the regional maps [30,36], the sedimentary and volcanic Autunian rocks are absent in the investigated area. The lowest interval of the SMV1 model comprises Lower Carboniferous strata that were restored as a result of long-lasting analysis, incorporating mapping results of Burzewski et al. [144] and Botor et al. [145].

The decision on K-1 spudding followed very recent completion, as well as partial merge and reprocessing of three 2D seismic surveys, which comprised 24 seismic lines. Based on these data, a structural and tectonic reinterpretation was completed by the PGNiG team. As a result, a large antiformal structure on the top surface of the Rotliegend complex was discovered. The K-1 well outcomes resulted in further changes in understanding of the local geology, as at its bottom, volcanic rocks of Autunian were found. Analysis of the results of the regional geothermal modeling shows that in the vicinity of the K-1 well, the heat flow density value may reach up to ca. 84 mW/m^2 and the temperature at a depth of 4000 m b.g.l. around 130 °C.

To prepare the new version of the structural model—the structural model in variant 2 (SMV2)—the authors used tectonic interpretation of the pre-Zechstein basement that was supplied by PGNiG. In addition, structural interpretation of seismic horizons completed by the PGNiG team was used, comprising: (1) the top of Rotliegend, (2) the top of Zechstein—the top of middle Buntsandstein, (3) the top of Muschelkalk, (4) the top of Keuper, (5) the top Middle Jurassic and (6) the top Jurassic horizons (Figure 9B). Additional seismic horizons were interpreted by the authors, to obtain a stratigraphic division of the structural framework relevant to the SMV1, which includes (7) the top of Triassic, (8) the top of Lower Jurassic and (9) the top of Lower Cretaceous. After adjustment of well logs to the seismic lines, the authors found out that further structural interpretations are possible involving: (10) the top Carboniferous, (11) the top of igneous Autunian complex, (12) the top Fluvial complex (intra Rotliegend), and (13) the top Eolian complex (intra Rotliegend) (Figure 9C). These data were supplemented with the new tectonic interpretation of the Zechstein complex, as the authors suggested the presence of a series of intra-salt thrusts (Figure 9C) that developed in the eastern wing of the Kłecko structure (probably they

also exist in the western flank of the salt pillow but to a minor extent). In addition, the tectonic setting of the Mesozoic cover was reinterpreted for modeling purposes. It involves large faults that form a complex tectonic graben system (Figures 9 and 10). According to thickness and structural variability, the Mesozoic fault system originated during the Late Cretaceous, post-Albian times.

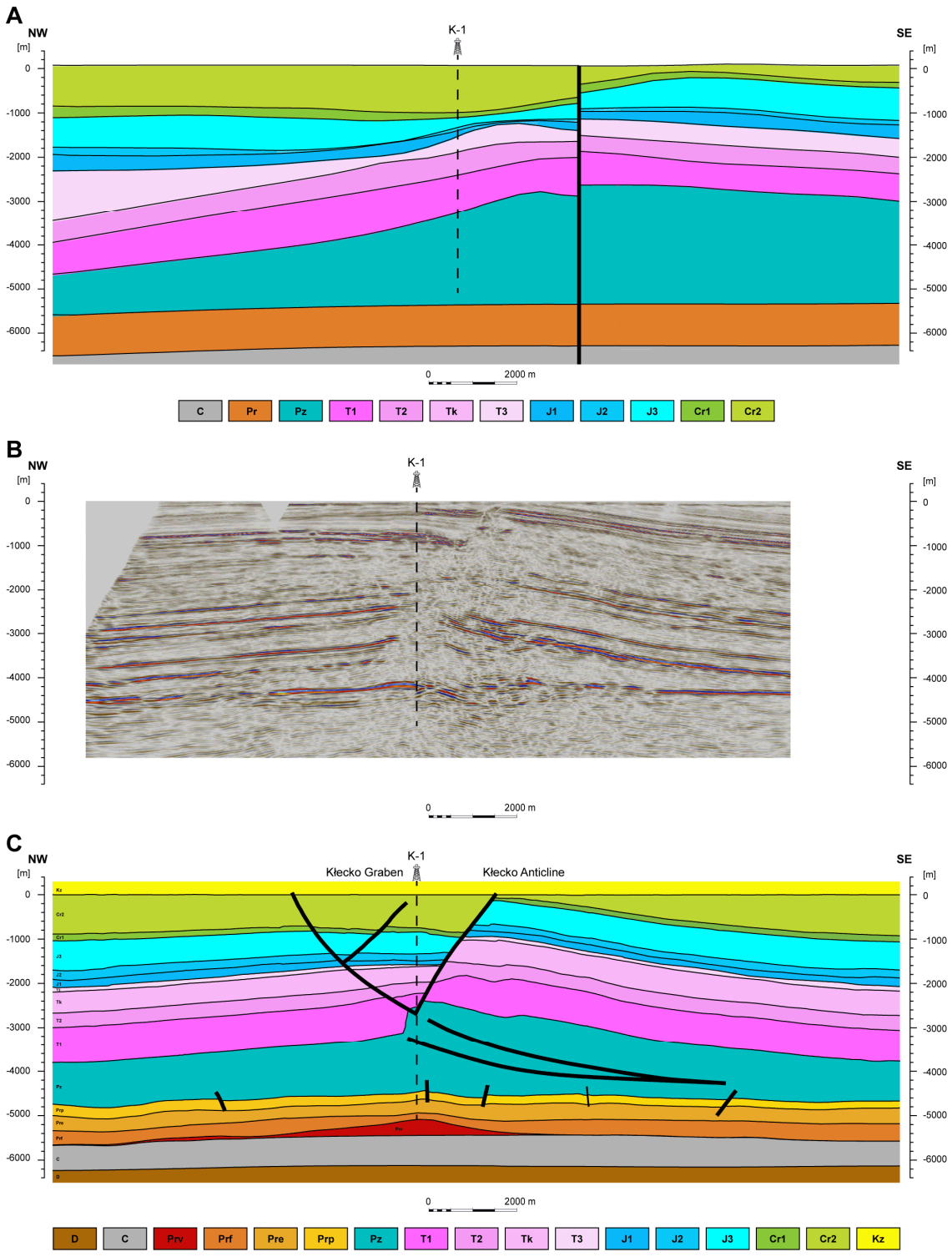

Figure 9. Structural interpretation of the Kłecko Anticline (**A**) structural model SMV1 along seismic

line 1; (**B**) seismic line 1 perpendicular to the anticline axis; (**C**) structural model in the new variant SMV2. Explanations: D—Devonian, C—Carboniferous, Pr—Rotliegend, Prv—Rotliegend volcanites, Prf—Rotliegend fluvial deposits, Pre—Rotliegend eolian deposits, Prp—Rotliegend playa, Pz—Zechstein, T1—Lower Triassic (Buntsandstein), T2—Middle Triassic (Muschelkalk), Tk—Keuper, T3—Upper Triassic, J1—Lower Jurassic, J2—Middle Jurassic, J3—Upper Jurassic, Cr1—Lower Cretaceous, Cr2—Upper Cretaceous, Kz—Cenozoic.

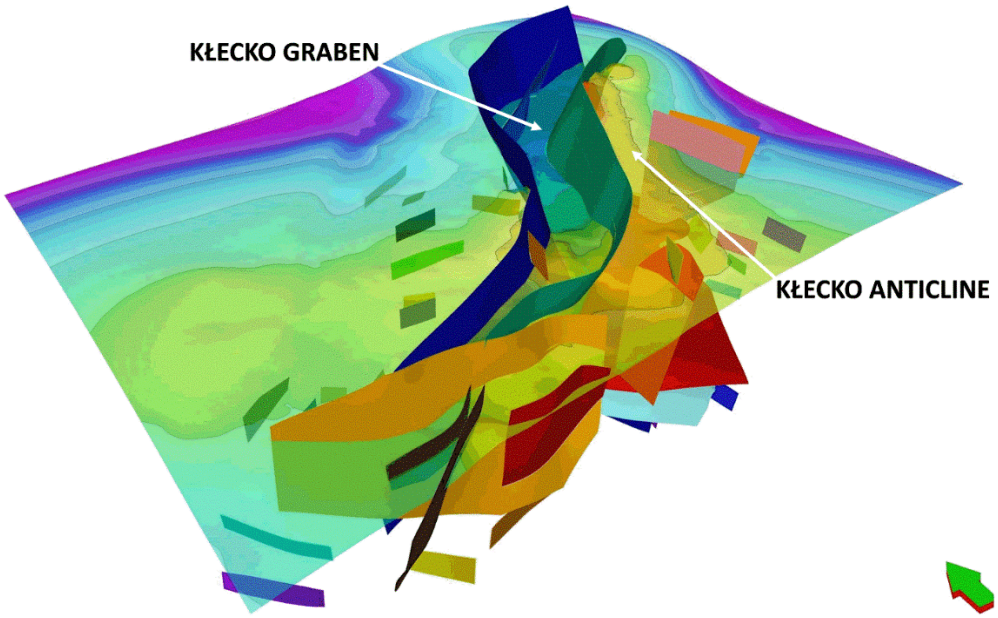

Figure 10. Spatial diagram of the tectonic variability at the background of the top Middle Jurassic surface (SMV2).

The graben involving all Mesozoic strata was formed over the salt pillow's crest in a transtensional regime, resulting from compressional deformation of underlying Zechstein salts. This late Cretaceous compression led to the development of the salt pillow and to gradual elevating of the eastern wing of the Kłecko Anticline. That process resulted in the erosion that created spatially restricted Albian subcrops below the Cenozoic base, east of the marginal fault of the Kłecko Graben (Figures 9 and 10).

The K-1 well is distant from other wells in the central part of the Mogilno-Łódź Trough, and it gives new stratigraphic control of that area. On the other hand, it is located in a very specific place, within the tectonic graben, and over the salt pillow. The stratigraphic column revealed by K-1 seems to be quite concordant with previous predictions for the Middle Jurassic to Upper Cretaceous strata. In general, it is also consistent with the assumptions regarding the Rotliegend successions. Considerable difference in the Permian interval is the unpredicted occurrence of volcanic rocks, which are located further to the east than previously mapped [28,37]. Shape and the thickness of the salt pillow also differs considerably from the older assumptions. The Lower Buntsandstein deposits drilled in K-1 are probably not representative for the zone, as eastern marginal fault of the Kłecko Graben causes reduction of the Lower and Middle Buntsandstein sequences.

The stratigraphic column of the K-1 well, together with the new structural model, delivers not only a new stratigraphic control over the area, but also gives novel insight into its thermal and petrophysical variability. Completed models revealed considerable discrepancy between regional approximations (SMV1) and models locally improved by K-1 results (SMV2). They can be the result of small-scale anomalies of the thermal field over the Autunian volcanic massive and/or the salt pillow of Zechstein, as well as of the geological evolution of the Kłecko Graben. Although the article focuses on the EGS reservoir within the Rotliegend, the authors make some references to the results of modeling its

overburden, as they well reflect some general tendencies of interaction between geological conditions and some typical behaviors (*sensu*: regularities of results) of stochastic modeling. In the case of low quantity and large distance between input wells, stochastic models give much more probable approximation of regional trends than any deterministic solution (Kriging, Moving Average), but they still differ from reality. Using models of temperature (TEMP), porosity (PHI) and shale volume (VSH), the authors illustrate the nature of the local anomalies compared to regional variability (Figures 11–16).

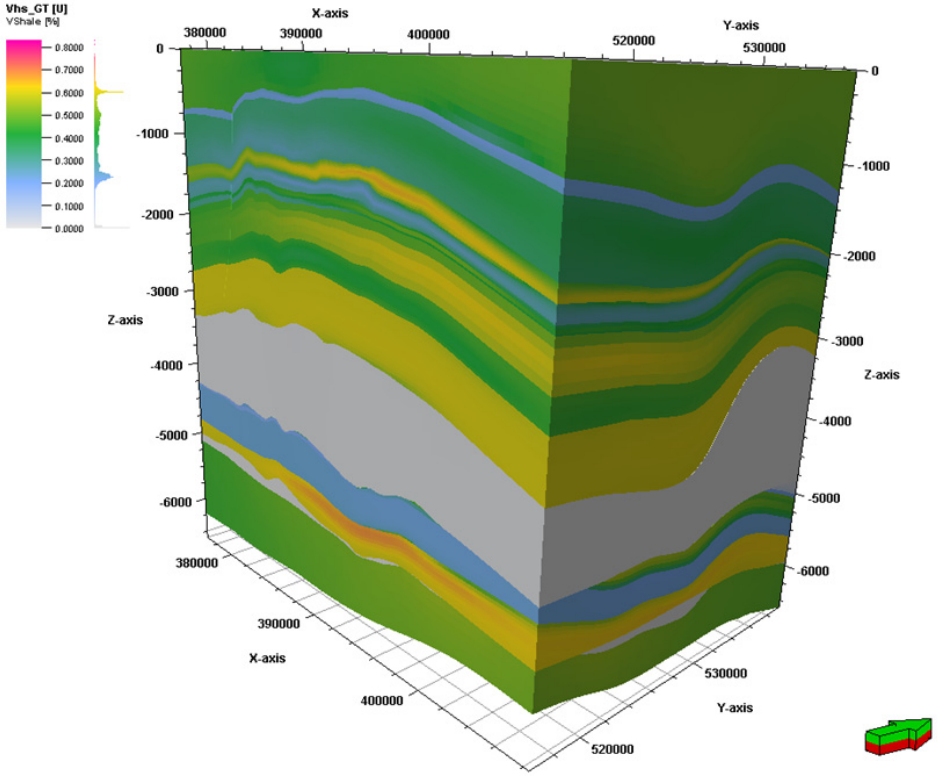

Figure 11. Spatial illustration of modeling results: model of shale volume (VSH) in variant 2.

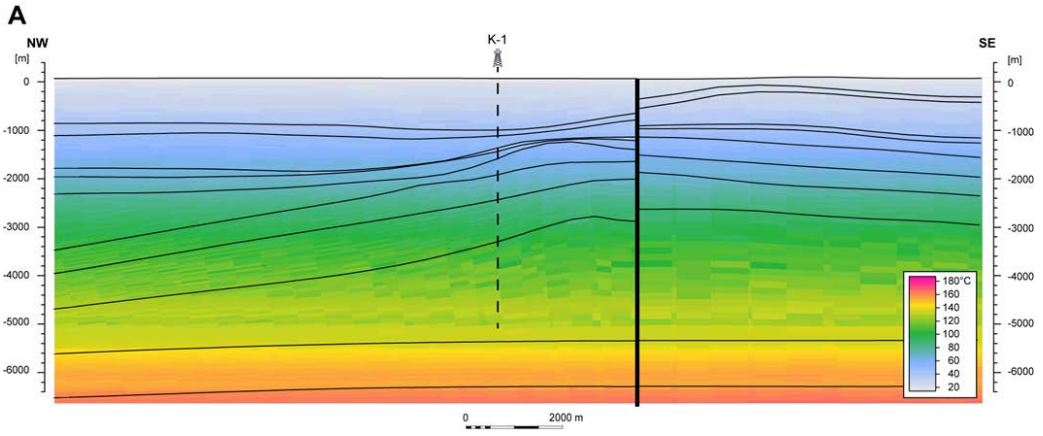

Figure 12. *Cont*.

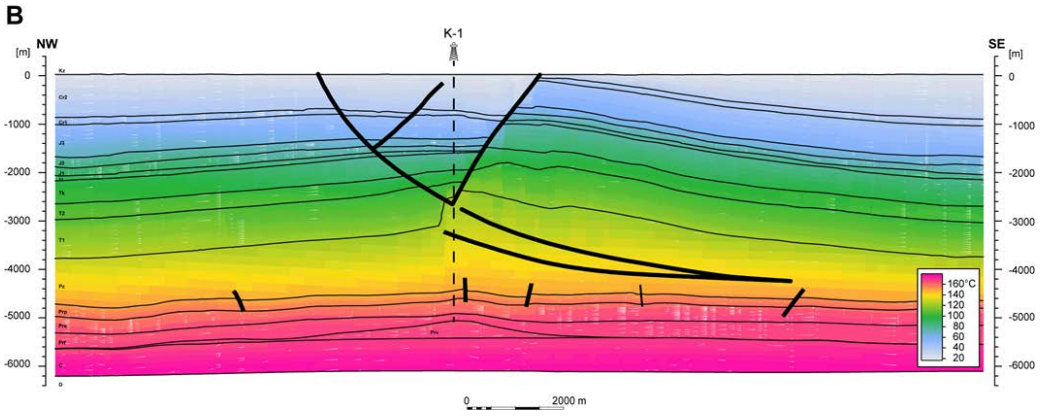

Figure 12. Distribution of the temperature along the NW–SE cross-sections: (**A**) upper part, SMV1; (**B**) lower part, SMV2.

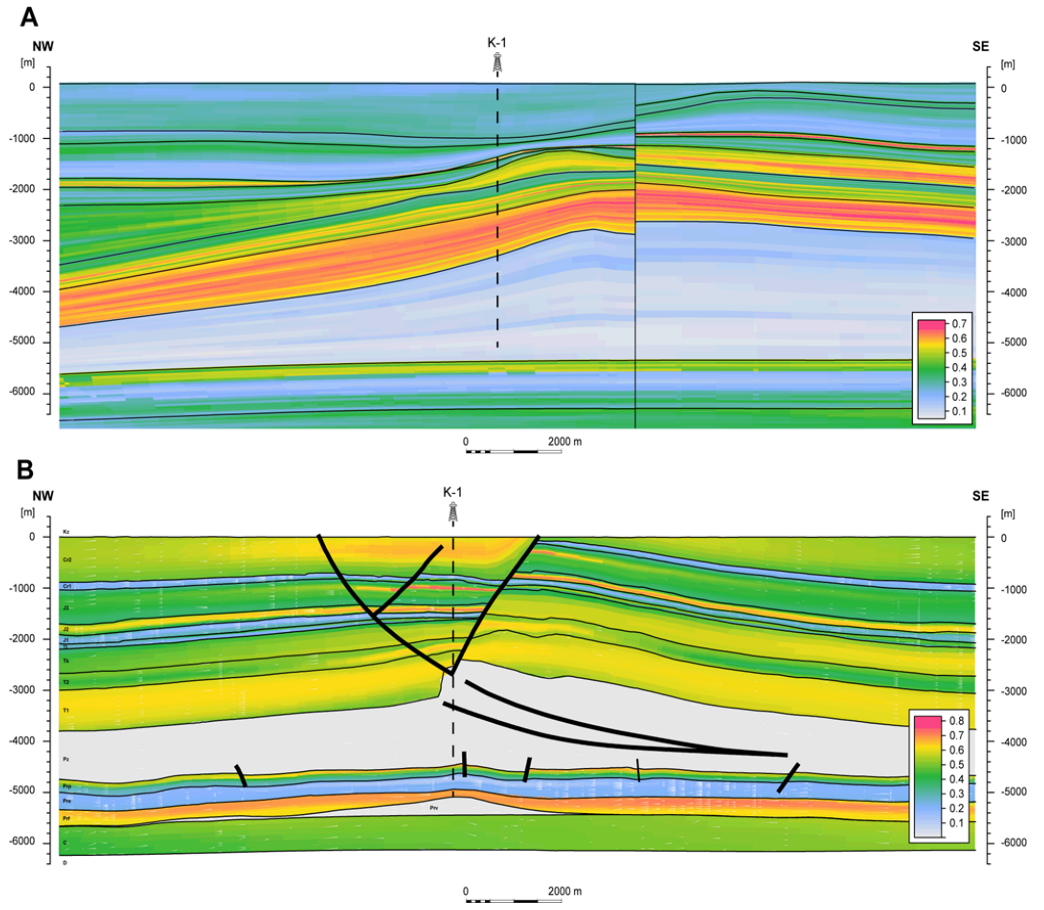

Figure 13. Distribution of the shale volume (VSH) along the NW–SE cross-sections: (**A**) upper part, SMV1; (**B**) lower part, SMV2.

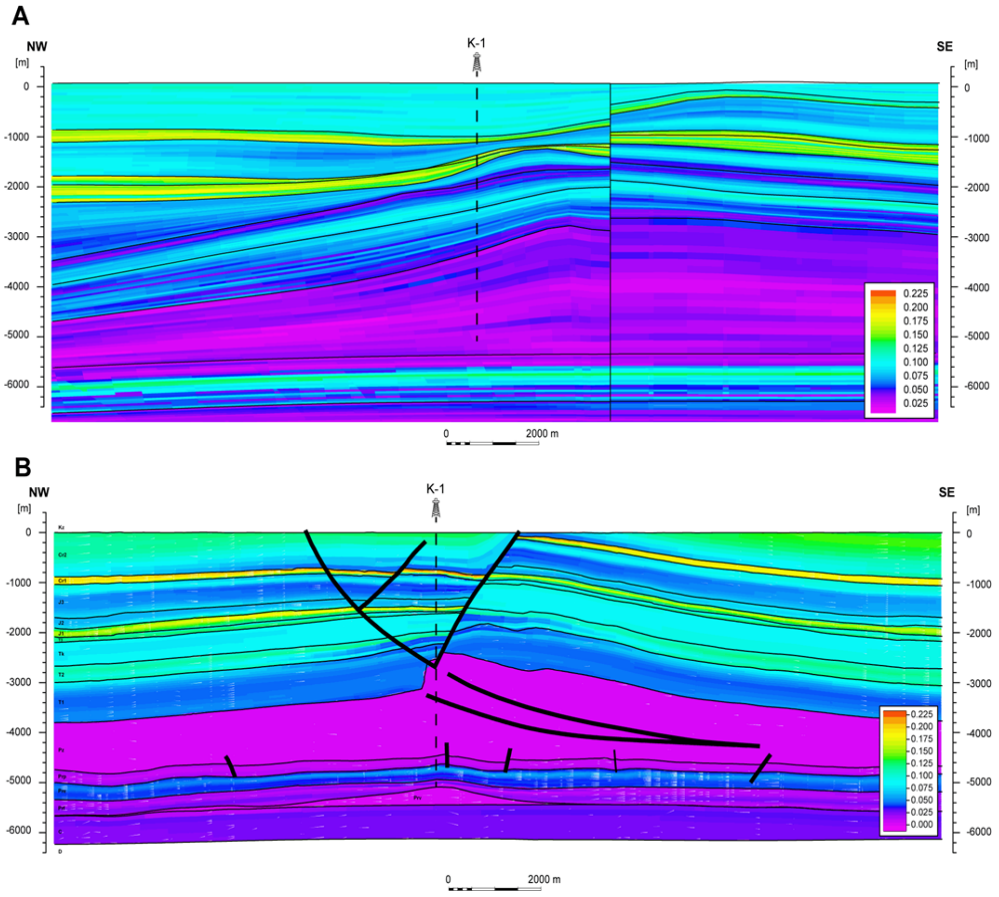

Figure 14. Distribution of the porosity (PHI) along the NW–SE cross-sections: (**A**) upper part, SMV1; (**B**) lower part, SMV2.

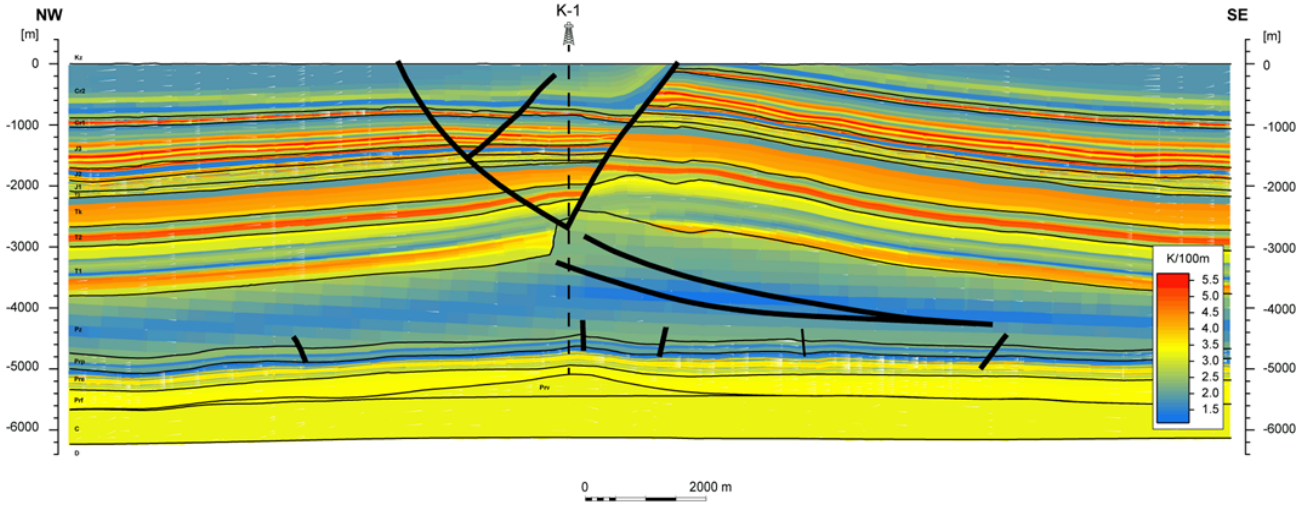

Figure 15. Distribution of the thermal gradient along the NW–SE cross-section (SMV2).

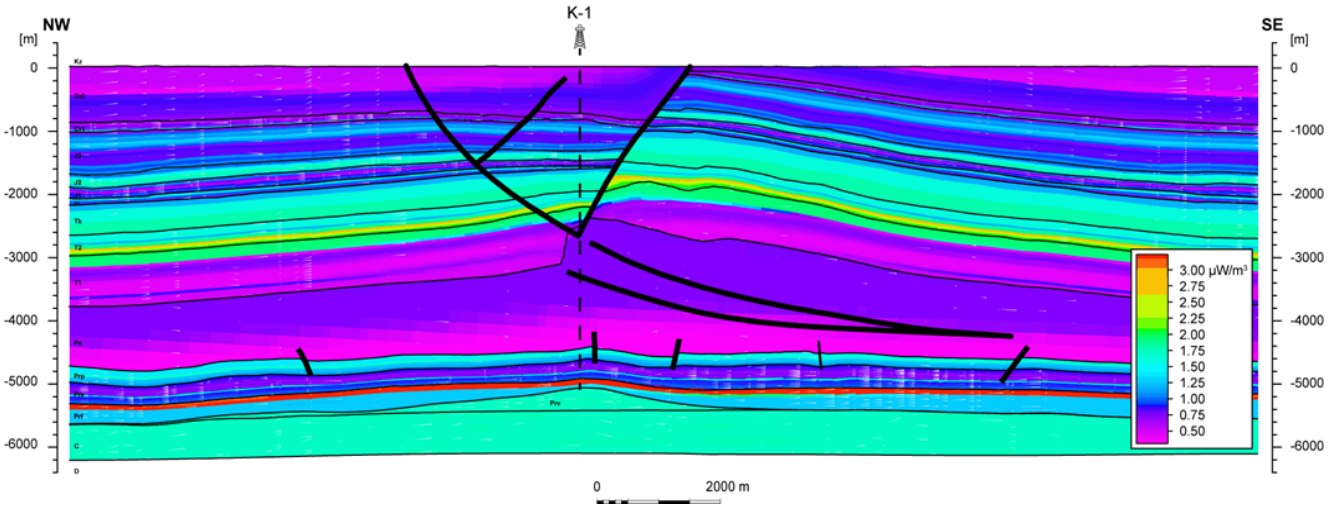

Figure 16. Distribution of the radiogenic heat production along the NW–SE cross-section (SMV2).

Temperature is a specific parameter, which shows smooth, wide-radius and depth-dependent spatial variability. The SMV1 and SMV2 of the temperature (Figure 12) represent it very well. In both solutions, depth increase is the most paramount parameter influencing temperature rise; however, in detail, both models differ significantly. Basically, the actual temperature in K-1 at particular depths is about 15 °C higher than expected, but its spatial variability is highly anomalous also due to local geology (Figure 12A,B). While the SMV1 model (Figure 12A) is very uniform in the entire area, and it barely reflects salt body influence on the spatial change of the temperature, the SMV2 shows abrupt temperature rise over the salt pillow crest and in the hanging wall of the Kłecko Graben (Figure 12A). Such variability demonstrates, on one side, high influence of the salt on the thermal field in its overburden, and on the other one, it can imply very young age of the salt structure and the graben. Approximately 10 km to the west from the eastern limit of the graben, the top of the Rotliegend and temperature decrease to the average regional trend (Figure 12B).

The comparison of average, minimum and maximum values, derived from the SMV1 and SMV2 models for the Rotliegend complex (Table 5, Figures 11–16), illustrates quantitative differences between the two cases. The average temperature is very comparable (151 °C vs. 152 °C) in both models for the Playa complex; however, the new model (SMV2) displays a lower average than the regional approximation (SMV1, Table 4). Only Eolian and Fluvial complexes show much better thermal conditions in the local (SMV2) model compared to regional approximation (SMV1) (Table 5).

The remaining modeled parameters show different, more geology-dependent, variability characteristics that represent rather planar trends, without obvious vertical constituents. An excellent example of such variability are the VSH and PHI models for the Zechstein complex. For both parameters, the regional variant (SMV1) shows considerable vertical variability, which in quantitative terms is very low, ranging from 0 to 0.2 for VSH (Figure 13A) and from 0 to 0.05 for PHI (Figure 14A). Values of these parameters in the local variants (SMV2), modified by K-1 results, are much lower and more uniform than SMV1, oscillating around 0% (VSH and PHI, Figures 13B and 14B). Presented discrepancies clearly illustrate the general tendency of the regional model's limitations, as, despite stochastic methods application, the forecasts of PHI and VSH are overestimated at the K-1 location. Results approximated by the SMV1 models reflect mainly random variability, conditioned with probability density curves of the parameters in Zechstein deposits. Partly, they are modified by input from wells located in the southern part of the FSM and in the MLT.

Table 5. Basic statistics of modeled parameters derived from models in variants SMV1 and SMV2 (min–max, avg.).

Parameter	Model	Playa	Eolian	Fluvial
PHI (%)	SMV1	1.10–12.45 (3.04)	1.27–15.76 (8.78)	0.97–11.06 (5.89)
	SMV2	0.43–3.19 (1.19)	0.00–8.85 (4.90)	0.26–3.70 (1.76)
V_{sh} (%)	SMV1	15.53–60.84 (47.40)	13.17–59.52 (21.56)	17.05–50.96 (32.57)
	SMV2	0.21–66.87 (32.44)	9.58–66.69 (22.49)	35.45–72.84 (60.97)
RHOB (g cm^{-3})	SMV1	2.44–2.77 (2.66)	2.41–2.75 (2.53)	2.50–2.74 (2.63)
	SMV2	2.58–2.77 (2.69)	2.50–2.69 (2.58)	2.26–2.86 (2.58)
Temp (°C)	SMV1	136.34–162.44 (151.29)	134.83–163.37 (150.93)	140.11–169.48 (155.04)
	SMV2	135.39–161.59 (152.31)	150.75–170.07 (160.84)	160.62–172.83 (166.34)
Thermal gradient (°C 100 m^{-1})	SMV1			
	SMV2	1.56–2.43 (2.08)	1.10–4.17 (2.83)	3.21–3.42 (3.37)
Radiogenic heat (μW m^{-3})	SMV1			
	SMV2	0.32–1.65 (1.27)	0.64–1.90 (0.89)	1.25–3.24 (1.85)

On the other hand, VSH and PHI values interpreted in the K-1 section for the Zechstein complex seem to be exceedingly low. The comparison presented above allows us to understand that some regional solutions, quite proper for the prospecting phase, must be revised during the exploration phase. Results of modeling obtained for the Rotliegend EGS reservoir, in both variants, were run separately for Playa, Eolian, and Fluvial associations (Table 5), that in the SMV1 models were distinguished as facies within the Rotliegend complex while in the SMV2 as sub complexes in the Rotliegend. Statistical comparison of the VSH shows that regional approximation (SMV1) matches quite well to local conditions (SMV2). For Playa and Eolian complexes, VSH is only slightly overestimated, while the lowermost Fluvial association is actually (SMV2) twice as abundant in shale as expected, displaying on average 32% and ~61% VSH, respectively (Table 5).

Porosity models of Rotliegend again disclose that the regional forecast (SMV1) was too optimistic. While in general, the vertical layout of porous and nonporous layers in both variants is similar, the quantitative description of PHI differs even more than 50% for all distinguished complexes (Table 5, Figure 14A,B). In both variants, estimated PHI is very low, but the results of the K-1 well imply that the SMV1 model underestimates the negative influence of burial on porosity. Despite porosity ranges and averages corresponding to older predictions [37], revised prognosis of the reservoir quality has to be diminished by about 50%. K-1 revision is very important, as at present it is the furthest to the north located well that reaches the Zechstein substratum.

Another parameter used in geothermal analyses is bulk density of rocks (RHOB), which is related to the lithology, porosity and burial depth of sedimentary rocks. Variability of RHOB is demonstrated in Table 6. Although the regional model (SMV1) of RHOB was built based on very little data, the differences between expectations and reality (SMV2) are fairly low, reaching only ±2.5%.

Table 6. Geothermal parameters of Rotliegend complexes in Kłecko Anticline for EGS system based on a 3D modeling and literature review, combined with the results of preliminary potential assessment.

Complex	Model	*Th*	*V*	ρ_{rock}	c_{rock}	T_{prod}	η_{th}	*HIP*	HIP_e	*TC*	TP_{th}	TP_{real}	TP_{low}
		m	$\times 10^8$ m^3	g cm^{-3}	J (kg·K)$^{-1}$	°C	10^{-2}	PJ	PJ	PJ	MW$_e$	kW$_e$	kW$_e$
Playa	SMV1	176.85	2.00	2.66	890	151	11.07	67.84	29.97	3.32	3.51	438.18	35.05
	SMV2	232.10	2.00	2.69	890	152	11.12	69.10	30.79	3.42	3.62	452.42	36.19
Eolian	SMV1	372.12	4.21	2.53	980	151	11.05	149.13	65.66	7.25	7.67	958.51	76.68
	SMV2	334.25	2.88	2.58	980	161	11.56	111.30	53.04	6.13	6.48	810.44	64.84
Fluvial	SMV1	206.83	2.34	2.63	900	155	11.30	82.84	37.12	4.18	4.42	552.30	44.18
	SMV2	326.31	2.81	2.58	900	166	11.85	103.38	51.15	6.06	6.41	800.80	64.06

Temperature gradient and radiogenic heat production have been spatially reconstructed in the SMV2 only, using K-1 well logs. These parameters add very precious information to local characteristics of the structure. At the base of the Kłecko Anticline a significant decrease of thermal gradient (Figure 15) and increase of temperature (Figure 12) is observed.

Similar behavior of these parameters has been described from almost all types of salt structures, except for salt pillows, from the German part of the Polish-German Permian Basin [146]. Practically in all structures analyzed by this team, isotherms at the base of the structure tend upwards. The maximum amplitude is located more or less in the center of the structure. An increase of temperature and decrease of the thermal gradient at the base of salt structures is a direct consequence of the high thermal conductivity of salts. In the topmost Playa complex a cooling effect is observed. It is probably responsible for the surprisingly low temperatures approximated by the SMV2 for the Playa complex as well (Table 5). Complexes located below Playa display a very stable and rather high temperature gradient ca. 3.5 °C 100 m^{-1}.

Within the Rotliegend sequence in the interval corresponding to the Fluvial facies, a noticeable increase of radiogenic heat (>3.2 μW m^{-2}) is observed (Figure 16). It is a direct result of an increase of natural gamma radioactivity (up to 260 API), that is expressed also in high values of interpreted VSH (up to 72%, Figure 13B). In general, the Rotliegend Playa facies within the Polish Permian Basin do not show such high clay volumes [37]. In the case of the Kłecko Anticline, an increase of gamma ray and radiogenic heat has to be caused by the rise of uranium content. The most probable explanation of this fact is an important fraction of volcanic rocks weathering products in the total mass of Playa facies rocks.

Because of the lack of appropriate core material, further attempts of explanation are more or less speculative, but the sequence may contain some tuff or tuffite intercalations. The concentration of minerals containing radioactive isotopes does not have to be a residuum of weathering of volcanic rocks building direct bedrock. It may also contain products of fluvial sedimentation or result of flooding events and related to their concentration of heavy minerals of volcanic origin.

The results presented above were then used in volumetric assessment of geothermal potential. They indicate that the Eolian complex in the K-1 area is an optimal one for the development of the EGS-type geothermal field.

Preliminary Results of EGS Geothermal Potential Assessment

A case study presented in this paper assumes the production of electricity, although combined heat and power (CHP) installation can also be considered. For the management and utilization of a geothermal reservoir following the objectives, the relevant reservoir temperature and sufficiently high production rates of geothermal fluids should at least be ensured. Despite the fact that the article does not address any issues related to the technology of heat extraction from the carrier fluid, the authors assume that the system will meet the cut-off criteria given in the literature for the initial economic viability of the EGS system [90,91]. This applies to a minimum fluid circulation rate of approx. 144 m^3 h^{-1} (40 Ls^{-1}) and a minimum working fluid temperature of approx. 160 °C. To obtain such

high productivity, the permeability of the supposed reservoir has to be stimulated by hydraulic fracturing. Hydraulic conductivity of the reservoir is determined by the rock mass permeability, which should be dominated by the fracture system rather than by low matrix permeability, estimated at 0.04 mD (an average value for the Rotliegend in the K-1 well).

In the model of heat exchange between the injected fluids and the rock mass, the parameters and shape of the zone that would be fractured were assumed. This zone defines a space for the accumulation of fluid migration between the wells and would be limited by poorly permeable or impermeable formations with permeability of 0.04 mD. The fractured zone is vertically limited by the rock properties and laterally by the extent of fracture. The assumed calculation reservoir has the shape of a cuboid with a total volume presented in Table 6.

Quantitative analysis focused on the determination of the amount of heat and/or power that can be produced from K-1 and requires an extensive multivariate analysis including reservoir simulations and modeling. This should be the subject of further work leading to precise assessment of technical reserves through the preparation of the feasibility study verifying the economic viability of the heat production from the K-1 EGS geothermal field.

For the preliminary calculation of technical potential, it is proposed to apply a simplified approach taking into account three different levels of R expressing: theoretical, realistic and pessimistic scenarios for geothermal energy extraction from the K-1 reservoir [133,136]:

- TP_{theory}—the maximum possible (theoretical) technical potential (R = 1.00);
- TP_{real}—realistic underground technical potential according to typical predictive reservoir engineering approaches and empirical practice expressing mean value of recovery factor (R = 0.125);
- TP_{low}—conservative approach on calculation of the technical potential, based on Beardsmore et al. [135] (R = 0.01).

Despite the fact that economic issues are not analyzed in this paper, for technological and economic reasons determining the use of hot dry rock technology, for the production of electricity, for the estimation of energy reserves of the K-1 reservoir, the target reservoir lying at a depth of 4.7–5.0 km was taken into account; its thickness is min. 300 m, and the temperature is around 160 °C. All the above listed parameters meet the criteria for EGS summarized in Table 2. Detailed information on the reservoir properties and assumed production parameters, combined with the results of the preliminary reserves assessment, is presented in Table 6.

Other assumptions taken into account when calculating reserves are:

- The influence of radiogenic heat on the thermal regeneration of the rock mass was not considered (radiogenic heat is important for the formation of thermal conditions of the rock mass only in the geological time scale);
- A homogeneous permeability of the fractured zone was assumed (the model was divided into fractures and a rock matrix, but the average value of permeability for the entire structure subjected to hydraulic fracturing was assumed, e.g., a single porosity model instead of dual porosity).

Estimations presented in Table 6 refer to geobodies differing in volumes, depths of burden, and petrophysical and thermal parameters. Hence, their direct interpretation does not show which facies (objective) is of the paramount prospectivity. Only in cases when this calculation is converted to a specific value referred to as 1 km^3 volume do results become easily comparable. Figures compiled in Table 7 show that energetic effectiveness of the Rotliegend described by new models is considerably higher than regional expectations (SMV1); in particular, Eolian and Fluvial complexes reveal very optimistic estimates of both HIPs and individual types of TPs.

Table 7. Specific geothermal resources of Rotliegend complexes in Kłecko Anticline assessed for models SMV1 and SMV2 in relation to the volume of 1 km^3.

Complex	Model	*sHIP*	*sHIP$_e$*	*sTC*	*sTP$_{th}$*	*sTP$_{real}$*	*sTP$_{low}$*
		PJ km^{-3}	**PJ km^{-3}**	**PJ km^{-3}**	**MW$_e$ km^{-3}**	**kW$_e$ km^{-3}**	**kW$_e$ km^{-3}**
Playa	SMV1	339.20	149.85	16.60	17.55	2190.90	175.25
	SMV2	345.50	153.95	17.10	18.10	2262.10	180.95
Eolian	SMV1	354.23	155.96	17.22	18.22	2276.75	182.14
	SMV2	386.46	184.17	21.28	22.50	2814.03	225.14
Fluvial	SMV1	354.02	158.63	17.86	18.89	2360.26	188.80
	SMV2	367.90	182.03	21.57	22.81	2849.82	227.97

Such a comparison of the SMV1 and SMV2 models discloses a serious improvement of available geothermal power, depending on rock type. Especially, a spectacular increase in available power refers to the Eolian complex, which accumulates 8.3% HIP more than expected, and each of TP parameters which are 19.1% higher than regional expectations. All these results are a bit confusing when interpreted individually, so they are discussed in a complex way later in the text.

8. Summary and Conclusions

The K-1 well, drilled in the central part of the NMT, was completed in 2008. Its results combined with interpretation of a new seismic survey acquired in its vicinity gave new understanding of the geology of the Kłecko Anticline. In this paper a new geothermal prospect and new method of geothermal exploration, based on comparison of vintage and new data as well as geomodeling, are described.

On the ground of local and regional scale data sets, two parametric models were completed. Based on the results of parametric modeling for the Rotliegend EGS reservoir, two scenarios (SMV1 and SMV2) of geothermal potential assessment were run, separately for Playa, Eolian and Fluvial associations.

The traditional approach to geothermal exploration within the Polish Lowlands is based on cartographic methods, which assume that maps form a synthesis of geological, petrophysical and thermal information [1,2]. Such an approach allows very good regional scale description but creates some radical simplifications. This method, developed from the 1990s, assumes substantial averaging of analyzed parameters as well as assigns thermal conditions to the tops of particular geothermal or stratigraphic complexes. The first variant of the model (SMV1) has a regional character and is based on a data set comparable to one in atlases [1,2]. The second model (SMV2) uses regional trends mapped in the SMV1, but its geometry reflects dramatic changes in structural geology, and thermal and petrophysical parameters are enriched with data collected in the K-1 well. Simple comparison of temperature mapped for the top of the Rotliegend [1,2] and by the SMV1 shows better correlation of the latter to the temperature measured in the well, and the SMV2 is fitted even better (139 °C, 151 °C and 152 °C, respectively). Because the SMV1 reflects trends of petrophysical and thermal properties distribution, typical for the MLT, part of the MPS and the northern part of FSM, it can be supposed that regional structural-parametric modeling gives satisfactory and optimal solutions. A more detailed analysis of obtained results negates this statement. Satisfactory modeled regional trend (SMV1) may give good approximation only in these places where thickness of particular stratigraphic sequences is typical for the entire basin.

In addition, statistical comparison of modeling results, performed for the total volume of the Playa, Eolian and Fluvial complexes, does not provide proper inference regarding geoenergetic prospectivity of particular facial complexes of the Rotliegend (Table 5). In a general comparison of results obtained from the local model, SMV2 indicates that the Eolian complex has a bit more favorable geothermal properties than the Fluvial and Playa sequences. Comparison of these results, combined with different values of HIP and

TP, suggests that local reinterpretation of environs of the K-1 well does not improve understanding of geothermal characteristics of the area (Table 5). It is because reserves (SMV2) accumulated in the Playa complex are almost identical as in the SMV1, moreover, in the case of the Eolian complex, they are about 15–19% lower. Scarcely, in the deepest Fluvial complex, in turn SMV2 reserves are about 30% larger than SMV1. Such comparison leads to a rather negative recommendation for commercial development, because it indicates as a prospective one the Fluvial complex, resting 5500 m b.s.l., with average clay content varying about 60% (Table 5), which makes it resistant for long distance fracturing treatment (Figure 13) required by EGS (Table 2).

Comparison of simple model statistics indicate the investigated area as rather non-prospective. It is a good example for illusory results of selective interpretation of statistical parameters. Total reserves presented in Table 6 remain in contradiction to average temperature determined for each complex. In the case of the Playa sequence, formation temperatures obtained in both the SMV1 and SMV2 models are similar (~151 °C and 152 °C, correspondingly), but the discrepancy for the Eolian complex is significantly higher, reaching 10 °C (150.1 °C vs. 160.1 °C), and in the case of the Fluvial complex it increases to 11 °C (155 °C vs. 166 °C). Specific geothermal resources that express the amount of heat stored in reference to 1 km^3 rock, show similar relations (Table 7). The parameters in the SMV2 model indicate a systematic increase of potential for each discussed complex. A significant relative increase of potential is related to the Eolian sequence, which accumulates 8.3% HIP more than expected and each of its TP parameters is 19.1% higher than regional expectations. These results indicate that it is an opportunity to produce electric power from EGS within the investigated area.

Considering geothermal potential per volume derived from the SMV2, it should be mentioned that the Fluvial complex has similar or even better parameters than the Eolian one, but is significantly less porous (avg. 1.76% vs. 4.90%; Table 5, Figure 14) and contains more clay minerals (avg. 60.97% vs. 22.50%; Table 5, Figure 13), which may diminish effectiveness of hydraulic fracturing. The Eolian complex composed of pure sandstones is definitely better for fracturing and rests 300 m shallower which reduces drilling costs. The average porosity of the Eolian complex interpreted from well logs (4.9%) is higher than 3%, a minimal requirement for commercial EGA (Table 2). The DST results during drilling of the K-1 well resulted in no flow, which may indicate that in this case interpreted porosity reflects total porosity. The higher content of bound water may favor the Eolian complex, because of the high heat capacity of water.

Analyzing thermal parameters of discussed Rotliegend complexes, some attention should be paid to radiogenic heat (RH). Within the sandy Eolian complex, RH varies between 0.5 to 0.75 μW m^{-3}, and in clay intercalation reaches up to 1.5 μW m^{-3}. In comparison, the Fluvial complex presents very high RH values, reaching even 3.4 μW m^{-3} (Figure 16). In the case of the presented analysis, radiogenic heat was determined as a function of shale content (VSH). Therefore, high VSH values are not typical for these facies within the Polish Permian Basin [37]. The authors suspect that such a rise of VSH, up to an extreme 72% (Table 5), may result from enrichment in radioactive minerals of volcanogenic origin and does not reflect real shale/clay content in the entire rock masses.

Analysis of the model of thermal gradient distribution within the Rotliegend strata indicates characteristic distribution of this parameter. The Playa complex and the top part of the Eolian complex are characterized by significantly lower thermal gradient (from 1.2 to 2.5 °C 100 m^{-1}) than deeper sequences of the Eolian and the Fluvial complexes (from 2.5 to 3.5 °C 100 m^{-1}). A similar cooling effect observed at the base of salt structures has been widely described [146–150]. It is common at the top of the Rotliegend within the German part of the Polish-German Permian Basin. It is related to intensive heat transfer through high-conductive Zechstein evaporites [146,149]. The distribution of the thermal anomalies (thermal gradient) within and around salt structures depends on their shape, but independent of the shape, all salt structures act as a channel for vertical heat transfer [146].

The changes in temperature gradients are proportional to the thickness of the salt sequence and the shape of the salt intrusion [150].

Analysis of the average heat flow also indicates visible thermal anomalies related to salt structures. Average heat flow at ground level within the Polish Permian Basin varies about 71 mW m^{-2} [72,151], in comparison within the German Permian Basin which varies about 63 mW m^{-2} [152], and in the environs of the K-1 well, according to Majorowicz's map [151], reaches 74 mW m^{-2}, while the heat flow determined in the K-1 was determined as ~84 mW m^{-2}. This indicates that the K-1 well is located within a local positive thermal anomaly. The Kłecko Anticline has the form of a salt pillow. This type of shape has the most preferable, from a geothermal exploration point of view, thermal properties distribution [146].

Furthermore, in areas with significant salt thickness (over several hundred meters, e.g., in the Polish Lowlands), detailed 3D models can identify the presence of appropriate conditions for the production of geothermal energy. Finally, the overlapping of thick salt layers, a suitable aquifer and demand for geothermal heat could outline favorable locations for geothermal development. The discussed methodology for assessing the geothermal potential is an important step towards the effective use of low-permeability (EGS) reservoirs for power generation or direct applications. The analysis presented above allowed the authors to draw the following conclusions:

- Regional scale 3D models can be used as a more precise tool for geothermal exploration than commonly applied solutions based on simple cartographic techniques;
- Presented here, subsalt thermal anomaly has not been precisely mapped in the regional approach (SMV1), because the distribution of temperature, typical for the entire basin, does not precisely reflect vertical anomalies within the vicinity of salt structures;
- Despite their imperfectness, regional models are indispensable for the creation of local scale models, because they allow external control of the parametric modeling process;
- All data used in this research have been collected during oil and gas exploration operations. All techniques and routines of data processing and analysis as well as applied software were adopted from the petroleum industry. Thus, the petroleum industry can be an important source of data and analytical tools for investigation of the Earth's thermal field and utilization of geothermal energy;
- Salt structures are potential objectives for geothermal exploration. The positive thermal anomalies at the top and above salt structures are a result of high thermal conductivity of salt. They may be emphasized by contact with low-conductive rocks, e.g., claystones;
- The changes of the thermal gradient are proportional to the salt thickness; the shape of the salt intrusion is also important;
- In Poland over ~100 salt structures have been mapped, a number of them may meet the criteria of being interesting objectives for geothermal exploration mentioned in Table 2;
- Further research of the Paleozoic formations is necessary for better understanding of high temperature resources and to indicate new opportunities for geothermal development in regions outside the areas of proven geothermal potential hosted in Mesozoic formations of the Polish Lowlands;
- Regional- to local-scale 3D models are very valuable for planning a deep geothermal installation. Because of the heterogeneity of the subsurface, basin geometry (especially around salt structures) and thermal properties, temperatures may deviate from the average geothermal gradient trend;
- The proposed methodology appears to be justified when a new well data set is used to verify 3D geological models in the salt structure zones. In particular, the discussed methods and models can be used to refine existing geothermal potential maps or to calibrate 3D parametric models used to assess both conventional and unconventional (EGS) geothermal potential;

- The general applicability of the proposed methodology makes it of interest for a broad range of applications in geothermal utilization as well as for CCS issues.

As a continuation of these findings, advanced research regarding geomechanics, well and formation engineering, and finally an economic analysis to quantify the financial benefits of the assessed potential of the Eolian complex should be completed for the presented case study, using modern concepts [153,154].

Author Contributions: Conceptualization, B.P. and R.K.; methodology, B.P., M.H. and R.K.; validation, G.M. and B.P.; resources, R.K. and G.M.; writing—original draft preparation, B.P., R.K. and M.H.; writing—review and editing, R.K., M.H., B.P. and G.M.; visualization, B.P., M.H. and R.K.; supervision, R.K. and B.P. All authors have read and agreed to the published version of the manuscript.

Funding: This research was funded by a statutory research program at the Faculty of Geology, Geophysics and Environmental Protection AGH University of Science and Technology in Krakow, Poland, statutory work No. 16.16.140.315/05.

Institutional Review Board Statement: Not applicable.

Informed Consent Statement: Not applicable.

Data Availability Statement: Publicly available datasets which were analyzed in this study can be found on: http://baza.pgi.gov.pl/ (accessed on 14 August 2021), other data are exclusive property of Polish Oil and Gas Company.

Acknowledgments: The authors are very indebted to the Polish Oil and Gas Company (PGNiG) for providing the core samples and geological data. We would like to thank E. Puskarczyk (AGH UST) for her help in the thermal conductivity measurements of the investigated samples, as well as S. Wysocki (AGH UST) for performing laboratory tests of selected rock samples in terms of their susceptibility to fracturing.

Conflicts of Interest: The authors declare no conflict of interest.

References

1. Górecki, W.; Hajto, M.; Papiernik, B.; Szczepański, A.; Kuźniak, T.; Kozdra, T.; Soboń, J.; Szewczyk, J.; Strzetelski, W.; Haładus, A.; et al. (Eds.) *Atlas of Geothermal Resources of Mesozoic Formations in the Polish Lowlands*; AGH University of Science and Technology in Krakow: Krakow, Poland; Ministry of Environment: Warsaw, Poland; NFEP&WM: Warsaw, Poland, 2006; p. 484. ISBN 978-83-88927-13-3. Available online: https://kse.agh.edu.pl/uploaded/AGH-Atlas_Geotermalny_Mezozoiku-2006.pdf (accessed on 14 August 2021).
2. Górecki, W.; Hajto, M.; Papiernik, B.; Szczepański, A.; Kuźniak, T.; Kozdra, T.; Soboń, J.; Szewczyk, J.; Strzetelski, W.; Haładus, A.; et al. (Eds.) *Atlas of Geothermal Resources of Paleozoic Formations in the Polish Lowlands*; AGH University of Science and Technology in Krakow: Krakow, Poland; Ministry of Environment: Warsaw, Poland; NFEP&WM: Warsaw, Poland, 2006; p. 240. ISBN 978-83-88927-14-0. Available online: https://kse.agh.edu.pl/uploaded/AGH-Atlas_Geotermalny_Paleozoiku-2006.pdf (accessed on 14 August 2021).
3. Zakrevsky, K.E. *Geological 3D Modelling*; EAGE Publications: Houten, The Netherlands, 2011; pp. 1–261.
4. Papiernik, B.; Michna, M. Methodology and results of digital mapping and 3D modelling of the Lower Palaeozoic strata on the East European Craton, Poland. *Ann. Soc. Geol. Pol.* **2019**, *89*, 405–427. [CrossRef]
5. Wójcicki, A.; Sowiżdżał, A.; Bujakowski, W. (Eds.) *Evaluation of Potential, Thermal Balance and Prospective Geological Structures for Needs of Unconventional Geothermal Systems (Hot Dry Rocks) in Poland*; Ministry of the Environment: Warsaw, Poland, 2013; pp. 1–246. (In Polish)
6. Karnkowski, P.H. Tectonic subdivision of Poland: Polish Lowlands. *Prz. Geol.* **2008**, *56*, 895–903. (In Polish)
7. Żelaźniewicz, A.; Aleksandrowski, P.; Buła, Z.; Karnkowski, P.H.; Konon, A.; Oszczypko, N.; Ślączka, A.; Żaba, J.; Żytko, K. *Regionalizacja Tektoniczna Polski*; Komitet Nauk Geologicznych PAN: Warsaw, Poland, 2011. (In Polish)
8. Pożaryski, W. The Middle European Caledonides—Wrenching orogen composed of terranes. *Prz. Geol.* **1990**, *38*, 1–9. (In Polish)
9. Guterch, A.; Wybraniec, S.; Grad, M.; Chadwick, R.A.; Krawczyk, C.M.; Ziegler, P.A.; Thybo, H.; de Vos, W. Crustal structure and structural framework. In *Petroleum Geological Atlas of the Southern Permian Basin Area*; Doornenbal, J.C., Stevenson, A.G., Eds.; EAGE Publications: Houten, The Netherlands, 2010; pp. 11–23.
10. Ziegler, P.A. *Geological Atlas of Western and Central Europe*, 2nd ed.; Shell Internationale Petroleum Maatschappij: London, UK; Geological Society Publishing House: Bath, UK, 1990; pp. 1–239.
11. Pharaoh, T.C.; Dusar, M.; Geluk, M.C.; Kockel, F.; Krawczyk, C.M.; Krzywiec, P.; Scheck-Wenderoth, M.; Thybo, H.; Vejbak, O.V.; Van Wees, J.D. Tectonic Evolution. In *Petroleum Geological Atlas of the Southern Permian Basin Area*; Doornenbal, J.C., Stevenson, A.G., Eds.; EAGE Publications: Houten, The Netherlands, 2010; pp. 25–57.

12. Krzywiec, P. Triassic-Jurassic evolution of the Pomeranian segment of the Mid-Polish Trough-basement tectonics and sedimentary patterns. *Geol. Q.* **2006**, *50*, 139–150.
13. Krzywiec, P. Structural inversion of the Pomeranian and Kuiavian segments of the Mid-Polish Polish Trough-lateral variations in timing and structural style. *Geol. Q.* **2006**, *50*, 151–168.
14. Jarosiński, M.; Poprawa, P.; Ziegler, P.A. Dynamic evolution of the Polish Platform. *Geol. Q.* **2009**, *53*, 3–26.
15. Mazur, S.; Malinowski, M.; Maystrenko, Y.; Gągała, Ł. Pre-existing lithospheric weak zone and its impact on continental rifting—The Mid-Polish Trough, Central European Basin System. *Glob. Planet. Chang.* **2021**, *198*, 103417. [CrossRef]
16. Mikołajczak, M.; Mazur, S.; Gągała, Ł. Depth-to-basement for the East European Craton and Teisseyre-Tornquist Zone in Poland based on potential field data. *Int. J. Earth* **2019**, *108*, 547–567. [CrossRef]
17. Kiersnowski, H.; Paul, J.; Peryt, T.M.; Smith, D.B. Facies, Paleogeography and Sedimentary History of the Southern Permian Basin in Europe. In *The Permian of Northern Pangea*; Scholle, P.A., Peryt, T.M., Ulmer-Scholle, D.S., Eds.; Springer: Berlin, Germany, 1995; pp. 119–136.
18. Stephenson, R.A.; Narkiewicz, M.; Dadlez, R.; van Wees, J.D.; Andriessen, P.A.M. Tectonic subsidence modelling of the Polish Basin in the light of new data on crustal structure and magnitude of inversion. *Sediment. Geol.* **2003**, *159*, 59–70. [CrossRef]
19. Dadlez, R.; Narkiewicz, M.; Stephenson, R.A.; Visser, M.T.M.; van Wees, J.D. Tectonic evolution of the Mid-Polish Trough: Modelling implications and significance for central European geology. *Tectonophysics* **1995**, *252*, 179–195. [CrossRef]
20. Leszczyński, K. Lithofacies evolution of the late Cretaceous basin in the Polish Lowlands. *Biul. Państwowego Inst. Geol.* **2010**, *443*, 33–54. (In Polish)
21. Narkiewicz, M.; Dadlez, R. Geological regional subdivision of Poland: General guidelines and proposed schemes of sub-Cenozoic and sub-Permian units. *Prz. Geol.* **2008**, *56*, 391. (In Polish)
22. Krzywiec, P. Triassic evolution of the Kłodawa salt structure: Basement-controlled salt tectonics within the Mid-Polish trough (central Poland). *Geol. Q.* **2004**, *48*, 123–134.
23. Krzywiec, P. Mesozoic and Cenozoic Evolution of Salt Structures within the Polish Basin—An overview. In *Salt Tectonics, Sediments and Prospectivity*; Special Publications; Alsop, G.I., Archer, S.G., Hartley, A.J., Grant, N.T., Hodgkinson, R., Eds.; Geological Society: London, UK, 2012; Volume 363, pp. 381–394.
24. Pożaryski, W. *The Early Alpine Laramide Epoch in the Platform Development East of the Fore Sudetic and Silesian-Cracovian Monoclines: Geology of Poland*; Wydawnictwa Geologiczne: Warszawa, Poland, 1977; pp. 351–416.
25. Marek, S.; Pajchlowa, M. (Eds.) *Permian and Mesozoic in Poland*; Prace Państwowego Instytutu Geologicznego: Warsaw, Poland, 1997; Volume 153, pp. 1–452.
26. Dadlez, R.; Marek, S.; Pokorski, J. *Atlas Paleogeograficzny Epikontynentalnego Permu i Mezozoiku w Polsce, 1:2,500,000*; Państwowy Instytut Geologiczny: Warsaw, Poland, 1998; pp. 1–7. (In Polish)
27. Peryt, T.M.; Geluk, M.C.; Mathiesen, A.; Paul, J.; Smith, K. Zechstein. Peri-Tethyan Rift/Wrench Basins and Passive Margins. In *Petroleum Geological Atlas of the Southern Permian Basin Area*; Doornenbal, J.C., Stevenson, A.G., Eds.; EAGE Publications: Houten, The Netherlands, 2010; pp. 123–147.
28. Doornenbal, J.C.; Abbink, O.A.; Duin, E.J.T.; Dusar, M.; Hoth, P.; Jasionowski, M.; Lott, G.K.; Mathiesen, A.; Papiernik, B.; Peryt, T.M.; et al. Introduction, Stratigraphic Framework and Mapping. In *Petroleum Geological Atlas of the Southern Permian Basin Area*; Doornenbal, J.C., Stevenson, A.G., Eds.; EAGE Publications: Houten, The Netherlands, 2010; pp. 1–9.
29. Pokorski, J. Formal lithostratigraphic subdivision proposed for the Rotliegendes of the Polish Lowlands. *Kwart. Geol.* **1981**, *25*, 41–58, (In Polish with English summary).
30. Pokorski, J. Rotliegendes lithostratigraphy in north-western Poland. *Bull. Pol. Acad. Sc.* **2008**, *36*, 99–108.
31. Karnkowski, P.H. Rotliegend lithostratigraphy in the central part of the Polish Permian Basin. *Geol. Q.* **1994**, *38*, 27–42.
32. Karnkowski, P.H. Origin and evolution of the Polish Rotliegend Basin. *PGI Spec. Pap.* **1999**, *3*, 1–93.
33. Kiersnowski, H. Depositional development of the Polish Upper Rotliegend Basin and evolution of its sediment source areas. *Geol. Q.* **1997**, *4*, 433–456.
34. Kiersnowski, H. *Depositional Architecture of the Rotliegend Basin in Poland, in Sedimentary Basins. Analysis of the Polish Lowlands*; Narkiewicz, M., Ed.; Prace Państwowego Instytutu Geologicznego: Warsaw, Poland, 1998; Volume 165, pp. 113–128.
35. Kiersnowski, H.; Buniak, A. Evolution of the Rotliegend Basin of northwestern Poland. *Geol. Q.* **2006**, *50*, 119–137.
36. Gast, R.E.; Dusar, M.; Breitkreuz, C.; Gaupp, R.; Schneider, J.W.; Stemmerik, L.; Geluk, M.C.; Geisler, M.; Kiersnowski, H.; Glennie, K.W.; et al. *Petroleum Geological Atlas of the Southern Permian Basin Area*; Doornenbal, J.C., Stevenson, A.G., Eds.; EAGE Publications: Houten, The Netherlands, 2010; pp. 101–122.
37. Papiernik, B.; Górecki, W.; Pasternacki, A. Preliminary results of 3D modeling of petrophysical parameters for tight gas prospecting in the Polish Rotliegend Basin. *Prz. Geol.* **2010**, *58*, 352–364. (In Polish)
38. Kiersnowski, H.; Buniak, A. Sand sheets interaction with aeolian dune, alluvial and marginal playa beds in Late Permian Upper Rotliegend setting (western part of the Poznań Basin, Poland). *Geol. Q.* **2016**, *60*, 771–800. [CrossRef]
39. Wagner, R.; Leszczyński, K.; Pokorski, J.; Gumulak, K. Palaeotectonic cross-sections through the Mid-Polish Trough. *Geol. Q.* **2002**, *46*, 293–306.
40. Czapowski, G. Geologia permskich struktur i złóż solnych w Polsce—Aktualny stan wiedzy i perspektywy zagospodarowania. *Prz. Geol.* **2006**, *54*, 301–302. (In Polish)

41. Wagner, R. *Stratigraphy and Development of the Zechstein Basin in the Polish Lowlands*; Prace Państwowego Instytutu Geologicznego: Warsaw, Poland, 1994; Volume 146, pp. 1–71.
42. Dadlez, R.; Marek, S.; Pokorski, J. *Geological Map of Poland without Cainozoic Deposits*; Polish Geological Institute: Warsaw, Poland, 2000.
43. Berthelsen, A. Mobile Europe. In *A Continent Revealed—The European Geotravers*; Blundell, D., Freeman, R., Mueller, S., Eds.; Cambridge University Press: Cambridge, UK, 1992; pp. 11–32.
44. Bachmann, G.H.; Kozur, H. The Germanic Triassic: Correlations with the international chronostratigraphic scale, numerical ages and Milankovitch cyclicity. *Hallesches Jahrb. Geowiss.* **2004**, *B26*, 17–62.
45. Pieńkowski, G. Facies criteria for delimitating the Zechstein/Buntsandstein and the Permian/Triassic boundary in Poland. *Zent. Für Geol. Paläontol.* **1991**, *4*, 893–912.
46. Szyperko-Teller, A.; Moryc, W. Evolution of the Buntsandstein sedimentary basin in Poland. *Kwart. Geol.* **1988**, *32*, 53–72. (In Polish)
47. Bachmann, G.H.; Geluk, M.C.; Warrington, G.; Becker-Roma, A.; Beutler, G.; Hagdorn, H.; Hounslow, M.W.; Nitsch, E.; Röhling, H.-G.; Simon, T.; et al. *Petroleum Geological Atlas of the Southern Permian Basin Area*; Doornenbal, J.C., Stevenson, A.G., Eds.; EAGE Publications: Houten, The Netherlands, 2010; pp. 149–173.
48. Marek, S.; Pajchlowa, M. *Epikontynentalny Perm i Mezozoik w Polsce*; Prace PIG: Warsaw, Poland, 1997; p. 153. (In Polish)
49. Pieńkowski, G. *The epicontinental Lower Jurassic of Poland*; Polish Geological Institute Special Papers; Polish Geological Institute: Warsaw, Poland, 2004; Volume 12, pp. 1–154.
50. Dadlez, R. *Epikontynentalne Baseny Sedymentacyjne w Polsce, od Dewonu po Kredę—Zależności Rozwoju od Budowy Skorupy Krystalicznej*; Prace Państwowego Instytutu Geologicznego: Warsaw, Poland, 1998; Volume 165, pp. 17–30. (In Polish)
51. Feldman-Olszewska, A. Jura Dolna. Miąższość. In *Atlas Paleogeograficzny Epikontynentalnego Permu i Mezozoiku w Polsce, 1:2,500,000*; Dadlez, R., Marek, S., Pokorski, J., Eds.; Wydaw. Kartograficzne Polskiej Agencji Ekologicznej: Warsaw, Poland, 1998; p. 36.
52. Dayczak-Calikowska, K.; Moryc, W. Evolution of sedimentary basin and paleotectonics of the Middle Jurassic in Poland. *Geol. Q.* **1988**, *31*, 117–136.
53. Niemczycka, T.; Brochwicz-Lewiński, W. Evolution of the Upper Jurassic sedimentary basin in the Polish Lowland. *Kwart. Geol.* **1988**, *32*, 137–155. (In Polish)
54. Dembowska, J. Systematization of lithostratigraphy of the Upper Jurassic in northern and central Poland. *Kwart. Geol.* **1979**, *23*, 617–630. (In Polish)
55. Lott, G.K.; Wong, T.E.; Dusar, M.; Andsbjerg, J.; Mönnig, E.; Feldman-Olszewska, A.; Verreussel, R.M.C.H. Jurassic. In *Petroleum Geological Atlas of the Southern Permian Basin Area*; Doornenbal, J.C., Stevenson, A.G., Eds.; EAGE Publications: Houten, The Netherlands, 2010; pp. 175–193.
56. Leszczyński, K. The Lower Cretaceous depositional architecture and sedimentary cyclicity in the Mid-Polish Trough. *Geol. Q.* **1997**, *41*, 509–520.
57. Leszczyński, K. The Upper Cretaceous carbonate-dominated sequence of the Polish Lowlands. *Geol. Q.* **1997**, *41*, 521–532.
58. Sokołowski, J. Warunki występowania wód geotermalnych w Polsce i program ich wykorzystania na Podhalu. *Tech. Poszuk. Geol. Geosynoptyka I Geoterm.* **1988**, *1–2*, 31–46. (In Polish)
59. Adamczyk, A.F.; Szczepański, A.; Szklarczyk, T. *Atlas Wód Geotermalnych Niżu Polskiego*; Objaśnienia tekstowe; Górecki, W., Ed.; Wyd. AGH: Krakow, Poland; ISE AGH: Krakow, Poland; Okręgowe Przedsiębiorstwo Geodezyjno-Kartograficzne: Krakow, Poland, 1990; p. 368. (In Polish)
60. Górecki, W.; Kuźniak, T.; Łapinkiewicz, A.; Maćkowski, T.; Strzetelski, W.; Szklarczyk, T.; Reicher, B. (Eds.) *Atlas Zasobów Energii Geotermalnej na Niżu Polskim*; ZSE AGH: Krakow, Poland; Towarzystwo Geosynoptyków GEOS: Krakow, Poland, 1995; p. 37. (In Polish)
61. Hajto, M.; Górecki, W. Energy potential of thermal waters in the Polish Lowland. *Biul. Państwowego Inst. Geol.* **2010**, *439*, 81–86. Available online: https://geojournals.pgi.gov.pl/bp/article/view/28856/20528 (accessed on 22 January 2021). (In Polish).
62. Hajto, M.; Górecki, W. The most prospective areas of use of thermal waters for heating purposes in the Polish Lowlands. *Biul. Państwowego Inst. Geol.* **2010**, *441*, 27–31. Available online: https://geojournals.pgi.gov.pl/bp/article/view/28871/20544 (accessed on 22 January 2021).
63. Sowiżdżał, A.; Papiernik, B.; Machowski, G.; Hajto, M. Characterization of petrophysical parameters of the Lower Triassic deposits in prospective location for Enhanced Geothermal System (central Poland). *Geol. Q.* **2013**, *57*, 729–744. [CrossRef]
64. Kępińska, B.; Barbacki, A.P.; Bielec, B.; Bujakowski, W.; Dendys, M.; Hołojuch, G.; Galos, K.; Kasztelewicz, A.; Kęsek, W.; Lankof, L.; et al. (Eds.) Geothermal Energy—A Basis for Low-Emission Space Heating Improving Living Conditions and Sustainable Development—Preliminary Studies for Selected Areas in Poland Study Visits. Report. 2017. Available online: http://www.eeagrants.agh.edu.pl/wp-content/uploads/2017/12/EEA-SVReport_GeoHeatPol-2017.pdf (accessed on 14 February 2021).
65. Hałaj, E.; Kępińska, B. Conjunctive uses of the geothermal water resources from Lower Cretaceous formations in the Mogilno–Łódź Trough, Poland. *Sustain. Water Resour. Manag.* **2019**, *5*, 1479–1494. [CrossRef]
66. Sowiżdżał, A.; Hajto, M.; Hałaj, E. Thermal waters of central Poland: A case study from Mogilno–Łódź Trough, Poland. *Environ. Earth Sci.* **2020**, *79*, 1–11. [CrossRef]

67. Papiernik, B.; Doligez, B.; Klimkowski, Ł. Structural and parametric models of the Załęcze and Żuchlów gas field region, Fore-Sudetic Monocline, Poland—An example of a general static modeling workflow in mature petroleum areas for CCS, EGR or EOR purposes. *Oil Gas Sci. Technol. Rev. D'ifp Energ. Nouv.* **2015**, *70*, 635–654. [CrossRef]
68. Moeck, I.S.; Beardsmore, G.A. New 'Geothermal Play Type' Catalog: Streamlining Exploration Decision Making. In Proceedings of the 39th Workshop on Geothermal Reservoir Engineering, Stanford, CA, USA, 24 February 2014; pp. 1–8.
69. Tester, J.W.; Anderson, B.J.; Batchelor, A.S.; Blackwell, D.D.; Dipippo, R.; Drake, E.M.; Garnish, J.; Livesay, B.; Moore, M.C.; Nichols, K.; et al. The Future of Geothermal Energy Impact of Enhanced Geothermal Systems (EGS) on the United States in the 21st Century. An Assessment by an MIT-Led Interdisciplinary Panel. 2006. Available online: https://energy.mit.edu/wp-content/uploads/2006/11/MITEI-The-Future-of-Geothermal-Energy.pdf (accessed on 22 January 2021).
70. Moeck, I.S. Catalog of geothermal play types based on geologic controls. *Renew. Sustain. Energy Rev.* **2014**, *37*, 867–882. [CrossRef]
71. Szewczyk, J.; Hajto, M. Heat Flow Versus Subsurface Temperatures in the Polish Lowlands. In *Atlas of Geothermal Resources of Mesozoic Formations in the Polish Lowlands*; Górecki, W., Hajto, M., Papiernik, B., Szczepański, A., Kuźniak, T., Kozdra, T., Soboń, J., Szewczyk, J., Strzetelski, W., Haładus, A., et al., Eds.; Ministry of Environment: Krakow, Poland; AGH University of Science and Technology: Krakow, Poland, 2006; pp. 143–151.
72. Szewczyk, J.; Gientka, D. Terrestrial heat flow density in Poland—A new approach. *Geol. Q.* **2009**, *53*, 125–140.
73. Nawrocki, J.; Becker, A. (Eds.) *Geological Atlas of Poland*; Państwowy Instytut Geologiczny—PIB: Warszawa, Poland, 2017; p. 170.
74. Majorowicz, J.; Wybraniec, S. New terrestrial heat flow map of Europe after regional paleoclimatic correction application. *Int. J. Earth Sci.* **2011**, *100*, 881–887. [CrossRef]
75. Majorowicz, J.; Polkowski, M.; Grad, M. Thermal properties of the crust and the lithosphere- asthenosphere boundary in the area of Poland from the heat flow variability and seismic data. *Int. J. Earth Sci.* **2019**, *108*, 649–672. [CrossRef]
76. Majorowicz, J.; Grad, M.; Polkowski, M. Terrestrial heat flow versus crustal thickness and topography—European continental study. *Int. J. Ter. Heat Flow Appl. Geotherm.* **2019**, *2*, 17–21. [CrossRef]
77. Plewa, S. *Rozkład Parametrów Geotermalnych na Obszarze Polski*; Wydaw. Centrum Podst. Prob. Gosp. Surowcami Mineralnymi i Energią PAN: Krakow, Poland, 1994; ISBN 83-86286-15-6. (In Polish)
78. Szewczyk, J.; Szczepański, A.; Haładus, A.; Kania, J.; Wagner, R.; Pokorski, J.; Hajto, M. Distribution of the Main Geothermal Parameters Referred to the Geological Setting in the Polish Lowlands. In *Atlas of Geothermal Resources of Mesozoic Formations in the Polish Lowlands*; Górecki, W., Hajto, M., Papiernik, B., Szczepański, A., Kuźniak, T., Kozdra, T., Soboń, J., Szewczyk, J., Strzetelski, W., Haładus, A., et al., Eds.; Ministry of Environment: Krakow, Poland; AGH University of Science and Technology: Krakow, Poland, 2006; pp. 198–255.
79. Majorowicz, J.; Šafanda, J. Lithosphere thickness from new heat-flow data of the Odra Variscan area, S-W Poland. *Pure Appl. Geophys.* **2018**, *175*, 4343–4354. [CrossRef]
80. Hałaj, E. Characteristics and sustainable utilization prospects of geothermal waters of the Liassic formations in the Mogilno–Łódź Trough, Poland. *Sustain. Water Resour. Manag.* **2018**, *5*, 1537–1553. [CrossRef]
81. Weber, J.; Born, H.; Pester, S.; Moeck, I. Geothermal Energy Use in Germany, Country Update 2015–2019. In Proceedings of the World Geothermal Congress, Melbourne, Australia, 19–25 April 2015; p. 15.
82. Blöcher, G.; Reinsch, T.; Henninges, J.; Milsch, H.; Regenspurg, S.; Kummerow, J.; Francke, H.; Kranz, S.; Saadat, A.; Zimmermann, G.; et al. Hydraulic history and current state of the deep geothermal reservoir Groß Schönebeck. *Geothermics* **2016**, *63*, 27–43. [CrossRef]
83. Zimmermann, G.; Tischner, T.; Legarth, B.; Huenges, E. Pressure-Dependent Production Efficiency of an Enhanced Geothermal System (EGS): Stimulation Results and Implications for Hydraulic Fracture Treatments. In *Rock Physics and Natural Hazards*; Pageoph Topical Volumes; Vinciguerra, S., Bernabé, Y., Eds.; Birkhäuser: Basel, Switzerland, 2009; pp. 1089–1106. [CrossRef]
84. Franz, M.; Barth, G.; Zimmermann, J.; Budach, I.; Nowak, K.; Wolfgramm, M. *Geothermal Resources of the North German Basin: Exploration Strategy, Development Examples and Remaining Opportunities in Mesozoic Hydrothermal Reservoirs*; Special Publications; Geological Society: London, UK, 2018; Volume 469, pp. 193–222. [CrossRef]
85. Jupe, A.J.; Bruel, D.; Hicks, T.; Hopkirk, R.; Kappelmeyer, O.; Kohl, T.; Kolditz, O.; Rodrigues, N.; Smolka, K.; Willis-Richards, J.; et al. Modelling of European prototype HDR reservoir. *Geothermics* **1995**, *24*, 403–419. [CrossRef]
86. Huenges, E.; Holl, H.; Bruhn, D.; Brand, W.; Saadat, A.; Moeck, I.; Zimmermann, G. Current State of the EGS Project Groß Schönebeck—Drilling into the Deep Sedimentary Geothermal Reservoir. In Proceedings of the European Geothermal Congress, Unterhaching, Germany, 30 May–1 June 2007; pp. 1–4.
87. Sausse, J.; Dezayes, C.; Genter, A. From Geological Interpretation and 3D Modelling to the Characterization of the Deep Seated EGS Reservoir of Soultz (France). In Proceedings of the European Geothermal Congress, Unterhaching, Germany, 30 May–1 June 2007; Available online: https://pangea.stanford.edu/ERE/pdf/IGAstandard/EGC/2007/059.pdf (accessed on 22 January 2021).
88. Brown, D.W.; Duchane, D.; Heiken, G.; Hriscu, V.T. *Mining the Earth's Heat: Hot Dry Rock Geothermal Energy*; Springer Science & Business Media: Berlin, Germany, 2012; p. 657.
89. Lu, S.M. A global review of enhanced geothermal system (EGS). *Renew. Sustain. Energy Rev.* **2018**, *81*, 2902–2921. [CrossRef]
90. Potter, R.; Robinson, E.; Smith, M. Method of Extracting Heat from Dry Geothermal Reservoirs. US Patent No. 3,786,858, 27 March 1972.

91. Williams, C.F.; Reed, M.J.; Mariner, R.H. *A Review of Methods Applied by the U.S. Geological Survey in the Assessment of Identified Geothermal Resources*; USGS Open File Report; US Department of Interior, US Geological Survey: Washington, DC, USA, 2008; Volume 1296, pp. 1–27.
92. Bujakowski, W.; Barbacki, A.; Miecznik, M.; Pajak, L.; Skrzypczak, R.; Sowizdzał, A. Modelling geothermal and operating parameters of EGS installations in the lower triassic sedimentary formations of the central Poland area. *Renew. Energy* **2015**, *80*, 441–453. [CrossRef]
93. Pazdro, Z.; Kozerski, B. *Hydrogeologia Ogólna*; Wydawnictwa Geologiczne: Warsaw, Poland, 1990. (In Polish)
94. Chadwick, A.; Arts, R.; Bernstone, C.; May, F.; Thibeau, S.; Zweigel, P. *Best Practice for the Storage of CO_2 in Saline Aquifers—Observations and Guidelines from the SACS and CO2STORE Projects*; British Geological Survey Occasional Publication, 14; British Geological Survey: Nottingham, UK, 2008; p. 267.
95. Barbier, E. Geothermal energy technology and current status: An overview. *Renew. Sustain. Energy Rev.* **2002**, *6*, 3–65. [CrossRef]
96. Garnish, J.D.; Batchelor, A.S.; Ledingham, P. Hot Dry Rock: Fringe Technology or Key Component? In Proceedings of the International Conference on Industrial Uses of Geothermal Energy, Reykjavik, Iceland, 2–4 September 1992; pp. 1–8.
97. Rybach, L. The Future of Geothermal Energy and its Challenges. In Proceedings of the World Geothermal Congress 2010, Bali, Indonesia, 25–29 April 2010; pp. 1–4. Available online: https://www.geothermal-energy.org/pdf/IGAstandard/WGC/2010/3109.pdf (accessed on 14 August 2021).
98. Jung, R. *EGS–Goodbye or Back to the Future, Effective and Sustainable Hydraulic Fracturing*; Jeffrey, R., Ed.; InTech: London, UK, 2013; ISBN 978-953-51-1137-5. Available online: https://www.intechopen.com/books/effective-and-sustainable-hydraulic-fracturing/egs-goodbye-or-back-to-the-future-95 (accessed on 14 August 2021). [CrossRef]
99. Breede, K.; Dzebisashvili, K.; Liu, X.; Falcone, G. A systematic review of enhanced (or engineered) geothermal systems: Past, present and future. *Geotherm. Energy* **2013**, 1–27. [CrossRef]
100. McDermott, C.I.; Randriamanjatosoa, A.R.L.; Tenzer, H.; Kolditz, O. Simulation of heat extraction from crystalline rocks: The influence of oupled processes on differential reservoir cooling. *Geothermics* **2006**, *35*, 321–344. [CrossRef]
101. Butler, S.J.; Sanyal, S.K.; Robertson-Tait, A. A Numerical Simulation study of the Performance of Enhanced Geothermal Systems. In Proceedings of the 29th Annual Workshop on Reservoir Engineering, Stanford, CA, USA, 26–28 January 2004.
102. Brigaud, F.; Chapman, D.S.; le Douaran, S. Estimating thermal conductivity in sedimentary basins using lithologic data and geophysical well logs. *AAPG Bull.* **1990**, *74*, 1459–1477.
103. Demongodin, L.; Pinoteau, B.; Vasseur, G.; Gable, R. Thermal conductivity and well logs: A case study in the Paris Basin. *Geophys. J. Int.* **1991**, *105*, 675–691. [CrossRef]
104. Midttømme, K.; Roaldset, E.; Aagaard, P. Thermal Conductivity of Argillaceous Sediments. In *Modern Geophysics in Engineering Geology*; McCann, D.M., Eddleston, M., Fenning, P.J., Reeves, G.M., Eds.; Geological Society of London: London, UK, 1997; Volume 12, pp. 355–363. [CrossRef]
105. Hartmann, A.; Rath, V.; Clauser, C. Thermal conductivity from core and well log data. *Int. J. Rock Mech. Min. Sci.* **2005**, *42*, 1042–1055. [CrossRef]
106. Gąsior, I.; Przelaskowska, A. Estimating thermal conductivity from core and well log data. *Acta Geophys.* **2014**, *62*, 785–801. [CrossRef]
107. Hajto, M.; Przelaskowska, A.; Machowski, G.; Drabik, K.; Ząbek, G. Indirect methods for validating shallow geothermal potential using advanced laboratory measurements from a regional to local scale—A Case study from Poland. *Energies* **2020**, *13*, 5515. [CrossRef]
108. Woodside, W.; Messmer, J.H. Thermal conductivity of porous media. II. Consolidated rocks. *J. Appl. Geophys.* **1961**, *32*, 1699–1706. [CrossRef]
109. Sass, J.H.; Lachenbruch, A.H.; Munroe, R.J. Thermal conductivity of rocks from measurements on fragments and its application to heat-flow determinations. *J. Geophys. Res.* **1971**, *76*, 3391–3401. [CrossRef]
110. Brigaud, F.; Vasseur, G. Mineralogy, porosity and fluid control on thermal conductivity of sedimentary rocks. *Int. J. Rock Mech. Min. Sci.* **1989**, *27*, A77. [CrossRef]
111. Tatar, A.; Mohammadi, S.; Soleymanzadeh, A.; Kord, S. Predictive mixing law models of rock thermal conductivity: Applicability analysis. *J. Pet. Sci. Eng.* **2020**, *197*, 107965. [CrossRef]
112. Lichtenecker, K. Die Herleitung des logarithmischen Mischungsgesetzes aus allgemeinen Prinzipien der stationären Strömung. *Phys. Z.* **1931**, *23*, 255–260.
113. Horai, K.-I.; Simmons, G. Thermal conductivity of rock-forming minerals. *Earth Planet. Sci. Lett.* **1969**, *6*, 359–368. [CrossRef]
114. Horai, K.-I. Thermal conductivity of rock-forming minerals. *Geophys. Res. Lett.* **1971**, *76*, 1278–1308. [CrossRef]
115. Čermák, V.; Rybach, L. Thermal Conductivity and Specific Heat of Minerals and Rocks. In *Geophysics—Physical Properties of Rocks*; Landolt-Börnstein-Group V Geophysics 1A (Subvolume A); Angenheister, G., Ed.; Springer-Verlag: New York, NY, USA, 1982; pp. 305–403.
116. Plewa, S. *Regionalny Obraz Parametrów Geotermicznych Obszaru Polski*; Prace Geofizyczne i Geologiczne: Warsaw, Poland; Wyd. Geofizyka i Geologia Naftowa: Warsaw, Poland, 1966; pp. 1–88. (In Polish)
117. Pasquale, V.; Verdoya, M.; Chiozzi, P. *Geothermics, Heat Flow in the Lithosphere*; Springer: Berlin, Germany, 2017; pp. 1–138.
118. Robertson, E.C. *Thermal Properties of Rocks*; Open-File Report; United States Department of the Interior, Geological Survey: Washington, DC, USA, 1988; Volume 88–441, pp. 1–106.

119. Kudrewicz, R. A 3D model of the thermal field within the Polish Carpathians and the Carpathian Foredeep (S Poland). *Geol. Q.* **2021**, *65*, 1–26. [CrossRef]
120. Fourier, J. *Theorie Analytique de la Chaleur*; Firmin Didot et Fils: Paris, France, 1822.
121. Fourier, J. Remarques generales sur les temperatures du globe terrestre et des espaces planetaires. *Ann. Chim. Phys.* **1824**, *27*, 136–167.
122. Bücker, C.; Rybach, L. A simple method to determine heat production from gamma-ray logs. *Mar. Pet. Geol.* **1996**, *13*, 373–375. [CrossRef]
123. Wygrala, B. Unconventional oil and gas—Efficient petrel/petromod workflows for exploration risk and resource assessments. *Prz. Geol.* **2014**, *62*, 825–841. (In Polish)
124. Wachowicz-Pyzik, A.; Pająk, L.; Papiernik, B.; Michna, M. The application of numerical modeling to geothermal investments. *Comput. Assist. Methods Eng. Sci.* **2015**, *22*, 385–396.
125. Dommisse, R.; Janson, X.; Male, F.; Price, B.; Payne, S.; Lewis, A. An Integrated, Multiscale Geomodel of the Northern Delaware Basin. In *SPE/AAPG/SEG Unconventional Resources Technology Conference*; OnePetro: Richardson, TX, USA, 2019. [CrossRef]
126. Ringrose, P.; Bentley, M. *Reservoir Model Design*; Springer Science+Business Media: Berlin, Germany, 2015; pp. 1–260.
127. Sowiżdżał, A.; Papiernik, B.; Machowski, G. The role of structural and parametric modelling in the process of selecting Enhanced Geothermal System location in sedimentary rocks. *Prz. Geol.* **2014**, *62*, 303–307.
128. Souche, L.; Lepage, F.; Iskenova, G. Volume Based Modeling—Automated Construction of Complex Structural Models. In Proceedings of the 75th EAGE Conference Exhib. Inc. SPE Eur., London, UK, 10–13 June 2013; pp. 10–13. [CrossRef]
129. Wang, B.; Bauer, S. Converting heterogeneous complex geological models to consistent finite element models: Methods, development, and application to deep geothermal reservoir operation. *Environ. Earth Sci.* **2016**, *75*, 1349. [CrossRef]
130. Papiernik, B.; Zając, J.; Michna, M.; Ząbek, G.; Machowski, G.; Kosakowski, P.; Poprawa, P.; Górecki, W. Application of Multiscale Spatial Modeling for Unconventional Hydrocarbon Assessment in the Central Part of Lublin Basin. In Proceedings of the X International GEOPETROL Conference, Oil and Gas Institute—National Research Institute, Research Papers, Zakopane, Poland, 19–22 September 2016; Volume 209, pp. 93–96. (In Polish).
131. Trumpy, E.; Botteghi, S.; Caiozzi, F.; Donato, A.; Gola, G.; Montanari, D.; Pluymaekers, M.P.D.; Santilano, A.; van Wees, J.D.; Manzella, A. Geothermal potential assessment for a low carbon strategy: A new systematic approach applied in southern Italy. *Energy* **2016**, *103*, 167–181. [CrossRef]
132. Van Wees, J.D.; Boxem, T.; Angelino, L.; Dumas, P. A Prospective Study on the Geothermal Potential in the EU. GEOELEC Report, Deliverable No. 2.5, 1–96. 2013. Available online: http://www.geoelec.eu/wp-content/uploads/2011/09/D-2.5-GEOELEC-prospective-study.pdf (accessed on 22 January 2021).
133. Blackwell, D.D.; Negraru, P.T.; Richard, M.C. Assessment of the enhanced geothermal system. Resource base of the United States. *Nat. Resour. Res.* **2006**, *15*, 283e308. [CrossRef]
134. Van Wees, J.D.; Kramers, L.; Kronimus, A.; Pluymaekers, M.P.D.; Mijnlieff, H.F.; Vis, G.-J. ThermoGISTM V1.0, Part II: Methodology. 2010. Available online: https://www.thermogis.nl/downloads/ThermoGISmanual_partII.pdf (accessed on 22 January 2021).
135. Beardsmore, G.; Rybach, L.; Blackwell, D.D.; Baron, C.A. Protocol for estimating the global potential for EGS. *Geotherm. Resour. Counc. Trans.* **2010**, *34*, 301–312.
136. Limberger, J.; Calcagno, P.; Manzella, A.; Trumpy, E.; Boxem, T.; Pluymaekers, M.P.D.; van Wees, J.-D. Assessing the prospective resource base for enhanced geothermal systems in Europe. *Geoth. Energ. Sci.* **2014**, *2*, 55–71. [CrossRef]
137. Chamorro, C.R.; García-Cuesta, J.L.; Mondéjar, M.E.; Linares, M.M. An estimation of the enhanced geothermal systems potential for the Iberian Peninsula. *Renew. Energy* **2014**, *66*, 1–14. [CrossRef]
138. Feng, Y.; Chen, X.; Xu, F.X. Current status and potentials of enhanced geothermal system in China: A review. *Renew. Sustain. Energy Rev.* **2014**, *33*, 214–223. [CrossRef]
139. Deibert, L.; Hjartarson, A.; McDonald, I.; McIlveen, J.; Thompson, A.; Toohey, B.; Yang, D. *The Canadian Geothermal Code for Public Reporting. Reporting of Exploration results, Geothermal Resources and Geothermal Reserves. Canadian Geothermal Energy Association*. 2010. Available online: https://www.cangea.ca/uploads/3/0/9/7/30973335/canadiangeothermalcodeforpublicreporting.pdf (accessed on 28 February 2021).
140. GEA 2010. New Geothermal Terms and Definitions. A Guide to Reporting Resource Development Progress and Results to the Geothermal Energy Association. 2010. Available online: https://nanopdf.com/download/new-geothermal-terms-and-definitions_pdf (accessed on 28 February 2021).
141. Van Wees, J.D.; Boxem, T.; Calcagno, P.; Lacasse, L.; Manzella, A. A Resource Assessment Protocol for GEO-ELEC. A Living Document Produced by the GEO-ELEC Project, 1–18. 2011. Available online: http://www.geoelec.eu/wp-content/uploads/2012/04/GEOELEC_RESOURCE-ASSESMENTPROTOCOL_v-16-dec-2011.pdf (accessed on 22 January 2021).
142. UNECE. Specifications for the Application of the United Nations Framework Classification for Fossil Energy and Mineral Reserves and Resources 2009 (UNFC-2009) to Geothermal Energy Resources. 2016. Available online: https://unece.org/DAM/energy/se/pdfs/UNFC/UNFC_GEOTH/UNFC.Geothermal.Specs.pdf (accessed on 22 January 2021).
143. IMGW. Climate Map for the Reference Period 1981–2010 in Poland. 2021. Available online: https://klimat.imgw.pl/pl/climate-maps/#Mean_Temperature/Yearly/1981-2010/1/Summer (accessed on 28 February 2021).

144. Burzewski, W.; Górecki, W.; Maćkowski, T.; Papiernik, B.; Reicher, B. Zasoby prognostyczne—Nieodkryty potencjał gazu ziemnego w polskim basenie czerwonego spągowca. *Geologia* **2009**, *35*, 123–128.
145. Botor, D.; Papiernik, B.; Maćkowski, T.; Reicher, B.; Kosakowski, P.; Machowski, G.; Górecki, W. Gas generation in Carboniferous source rocks of the Variscan Foreland Basin: Implications for a charge history of Rotliegend deposits with natural gases. *Ann. Soc. Geol. Pol.* **2013**, *83*, 353–383.
146. Fromme, K.; Michalzik, D.; Wirth, W. Das geothermische Potenzial von Salzstrukturen in Norddeutschland. *Z. Dt. Ges. Geowiss.* **2010**, *161*, 323–333.
147. Yu, Z.; Lerche, I.; Lowrie, A. Thermal impact of salt: Simulation of thermal anomalies in the Gulf of Mexico. *Pure Appl. Geophys.* **1992**, *138*, 181–192. [CrossRef]
148. Selig, F.; Wallick, G.C. Temperature distribution in salt domes and surrounding sediments. *Geophysics* **1966**, *31*, 346–361. [CrossRef]
149. Fuchs, S.; Förster, A. Rock thermal conductivity of Mesozoic geothermal aquifers in the northeast German basin. *Chem. Erde Geochem.* **2010**, *70*, 13–22. [CrossRef]
150. Daniilidis, A.; Herber, R. Salt intrusions providing a new geothermal exploration target for higher energy recovery at shallower depths. *Energy* **2017**, *118*, 658–670. [CrossRef]
151. Majorowicz, J.; Grad, M. Differences between recent Heat Flow Maps of Poland and deep thermo-seismic and tectonic age constraints. *Int. J. Ter. Heat Flow Appl. Geotherm.* **2020**, *3*, 11–19. [CrossRef]
152. Kaltschmitt, M.; Huenges, E.; Wolff, H. (Eds.) *Energie aus Erdwärme—Geologie, Technik und Energiewirtschaft*; Deutscher Verlag für Grundstoffindustrie: Stuttgart, Gemany, 1999; pp. 1–265.
153. Cui, G.; Ning, F.; Dou, B.; Li, T.; Zhou, Q. Particle migration and formation damage during geothermal exploitation from weakly consolidated sandstone reservoirs via water and CO_2 recycling. *Energy* **2022**, *240*, 122507. [CrossRef]
154. Cui, G.; Wang, W.; Dou, B.; Liu, Y.; Tian, H.; Zheng, J.; Liu, Y. Geothermal energy exploitation and power generation via a single vertical well combined with hydraulic fracturing. *J. Energy Eng.* **2022**, *148*, 04021058. [CrossRef]